



HAL
open science

Internal wave-driven mixing: governing processes and consequences for climate

Caitlin B. Whalen, Casimir de Lavergne, Alberto C. Naveira Garabato, Jody M. Klymak, Jennifer A. Mackinnon, Katy Sheen

► To cite this version:

Caitlin B. Whalen, Casimir de Lavergne, Alberto C. Naveira Garabato, Jody M. Klymak, Jennifer A. Mackinnon, et al.. Internal wave-driven mixing: governing processes and consequences for climate. Nature Reviews Earth & Environment, 2020, 1 (11), pp.606-621. 10.1038/s43017-020-0097-z . hal-03004969

HAL Id: hal-03004969

<https://hal.science/hal-03004969>

Submitted on 9 Oct 2021

HAL is a multi-disciplinary open access archive for the deposit and dissemination of scientific research documents, whether they are published or not. The documents may come from teaching and research institutions in France or abroad, or from public or private research centers.

L'archive ouverte pluridisciplinaire **HAL**, est destinée au dépôt et à la diffusion de documents scientifiques de niveau recherche, publiés ou non, émanant des établissements d'enseignement et de recherche français ou étrangers, des laboratoires publics ou privés.

24 with the global climate system, with the aim of inspiring future work on internal wave-driven mixing
25 across all scales.

26 **2. Key Points**

- 27 • Tides, winds, and geographic currents can generate oceanic internal waves and as a result
28 are major sources of energy for the internal wave field.
- 29 • Interactions between internal waves and topography, currents, or other internal waves can
30 transfer energy to smaller spatiotemporal scales. However, how these processes combine to
31 yield the observed internal wave environment is not well understood.
- 32 • Eventually, internal waves can become unstable, causing them to turbulently dissipate en-
33 ergy and mix water across density classes, thereby altering ocean dynamics.
- 34 • The location and timing of internal wave generation, energy transfer to smaller scales, and
35 subsequent turbulent dissipation conspire to form the continually evolving global distribu-
36 tion of mixing from internal waves.
- 37 • The global climate is shaped by the magnitude and geography of internal wave mixing.
38 Future work can provide an integrated understanding of internal wave mixing in an evolving
39 climate system.

40 **3. Introduction**

41 Just like surface waves exist along the sharp density interface at the boundary between the
42 ocean and atmosphere, internal waves are often supported by smooth vertical gradients in density
43 far beneath the ocean's surface. Internal waves often become unstable and break, generating
44 turbulence. A single patch of ocean turbulence from an unstable internal wave dissipates energy,
45 alters the stratification by mixing water of different densities, and thereby plays an important
46 dynamical role in the local environment. Close to the surface and the seafloor, instabilities that

47 are unrelated to internal waves often dominate the production of turbulence [1, 2]. However, away
48 from surface and bottom boundaries, internal waves are the primary cause of turbulent mixing.

49 In aggregate, such small (centimeter to meter) scale mixing from internal waves is essential for
50 sustaining the global overturning circulation [3, 4, 5, 6] and closing the global ocean energy budget
51 [7, 8, 9]. Internal wave-driven mixing is also important for transporting tracers such as nutrients,
52 greenhouse gases, and carbon [10, 11, 12, 13, 14] around the planet, thus shaping the biological
53 landscape of the global ocean [15]. Mixing from internal waves varies substantially in both space
54 and time throughout the ocean. Its distribution is set by the diverse processes that generate internal
55 waves (including tides, winds or larger-scale geostrophic ocean currents), alter their propagation,
56 and facilitate their dissipation. The complexity of the internal wave lifecycle leading to turbulent
57 mixing has inspired many avenues of inquiry.

58 Early work focused on understanding the local physics of internal waves [16, 17, 18, 19], and
59 hypothesized that the mixing caused by these waves has global implications [20]. More recent
60 efforts to study internal wave-driven mixing have advanced our understanding of the local physics,
61 and linked internal wave processes inducing mixing that are disparate in space and time to a
62 holistic view of the entire ocean system. Recent reviews have focused specific threads of areas of
63 rapid development, including parameterization of internal wave-driven mixing in climate models
64 [21], and reported on the current understanding of internal waves near the inertial frequency [22].

65 This review will adopt a wider perspective by targeting internal wave physical processes and
66 how they contribute to setting the complex spatio-temporal structure of mixing in the ocean. After
67 describing the physics of mixing due to breaking internal waves, the review will examine internal
68 wave energy pathways, categorized according to the waves' energy source. Subsequently, the review
69 will outline implications of internal wave-driven mixing for global ocean circulation and climate,
70 emphasizing knowledge frontiers.

4. Physics of Mixing from Internal Waves

Internal waves are ubiquitous in the stratified ocean interior. Flow along the uneven seafloor, perturbations at the base of the mixed layer, or fluctuating ocean currents can all generate internal waves (Figure 1). The signature of the generation mechanism is imprinted on the internal waves' spatial and temporal characteristics, leading to internal waves that have horizontal scales of order 0.1-100 kilometers and vertical scales that range from meters to scales comparable to the ocean depth. The structure and behaviour of internal waves is often modeled using orthogonal modes [G] [23]. Waves with vertical scales comparable to the ocean depth have small mode numbers and are called 'low-mode internal waves', whereas waves with smaller vertical scales have large mode numbers and are called 'high-mode internal waves' [23]. The high-mode internal waves can often occur in packets with vertical extents of hundreds of meters. The horizontal group velocity (that is, the velocity of energy propagation) is inversely proportional to mode number, such that low-mode wave energy travels faster than high-mode energy. The frequencies of internal waves are roughly bounded on the high end by the buoyancy frequency [G] (N) and on the low side by the local Coriolis frequency [G] (that is, the inertial frequency, f). A single generation event generally produces a spectrum of waves with a range of spatial scales and frequencies.

Once the internal waves are generated, they propagate throughout the ocean, interacting with other waves, currents and topography in ways that lead to a transfer of energy across scales and a loss of coherence of the initial waves. Far from boundaries, wave-wave interactions are a major process that can transfer energy to smaller scales [24, 25, 26]. Wave-wave interactions involve a resonance or near-resonance between three or more internal waves, causing an exchange of energy between waves of different wavelengths and frequencies that can shift energy to waves on smaller spatiotemporal scales. A particularly efficient class of wave-wave interactions occurs when one or more of the high-mode internal waves have near-zero group velocity, allowing sustained growth due

95 to energy transfer with a low-mode wave of approximately double their frequency, through a process
96 known as parametric subharmonic instability [27, 28, 29]. Additionally, as internal waves propagate
97 through variable background velocity and stratification, their length scales and group velocity may
98 change. For example, substantial variability in the background field can induce a rapid decrease
99 in the vertical scale of the wave, referred to as a critical layer [30, 31, 32]. Close to the seafloor,
100 the dominant dynamics change, and the scattering of internal waves off rough topographic features
101 or continental slopes is the most important class of processes that can turn larger-scale waves into
102 smaller-scale ones.

103 Ultimately, internal waves cascade to small enough scales to trigger a mixture of shear and
104 convective instabilities, turbulently dissipating wave energy through the internal wave equivalent
105 of breaking [33]. For example, shear instabilities can extract kinetic energy from an internal wave,
106 inducing turbulence (for example, Figure 2a-b). Alternatively, an internal wave can also generate
107 turbulence through convective instability that occurs when denser water at the wave crest moves
108 over lighter water [34], producing turbulence by extracting potential energy from the wave (for
109 example, Figure 2c-d). The turbulence generated by internal waves in the open ocean is typically
110 patchy and intermittent, exhibiting spatial scales of order 0.1-100 m and time scales of minutes to
111 hours [35, 36]. Where and when an internal wave dissipates energy depends strongly on the mode
112 number of the wave, since the mode sets the vertical scale, group velocity, and susceptibility to
113 wave-wave interactions [37, 38].

114 Breaking internal waves create turbulent kinetic energy, which is then either lost to viscous
115 dissipation (at a rate ϵ) [G] or to work against the ocean's density gradients (expressed as a buoyancy
116 flux, J_b). The two are related by the flux coefficient $\Gamma = J_b/\epsilon$ [39, 40]. The buoyancy flux can be
117 expressed as a down-gradient mixing of density at a rate given by a diapycnal diffusivity [G] K , so

118 that $J_b = KN^2$, or

119 (1)
$$K = \frac{\Gamma\epsilon}{N^2}.$$

120 K is the variable ultimately needed to model vertical mixing of oceanic tracers. Realistic repre-
121 sentation of internal wave-driven mixing thus requires knowledge of the turbulent kinetic energy
122 dissipation rate ϵ and of the flux coefficient Γ [39]. In open-ocean internal wave environments,
123 the flux coefficient is often close to 0.2; however a number of studies do indicate that Γ can vary
124 throughout the ocean [40].

125 There are two primary observational approaches to estimate the intensity of turbulence associated
126 with internal waves: direct and indirect methods. Spectra of oceanic shear on centimeter scales
127 measured with microstructure probes can be compared directly to theoretical turbulence spectra
128 and used to calculate ϵ [41, 42]. Indirect methods use finescale measurements (on 1-10 m scales) that
129 are analogously compared to internal wave spectra via the adoption of more assumptions, in order to
130 provide the turbulent kinetic energy dissipation rate expected from an observed internal wave field
131 [43, 44, 45, 46]. Finescale measurements generally agree with microstructure measurements within
132 a factor of 2-3 [45, 47, 48] in the open-ocean thermocline when they are compared on equivalent
133 time and length scales, which is considered a strong agreement, since dissipation rates vary over
134 many orders of magnitude.

135 Next, we move from describing studies that target the physics of internal wave generation,
136 propagation and breaking, to adopting a global perspective of the distribution and implications of
137 internal wave-driven mixing.

138 **5. Global Internal Wave Energy Budget**

139 Knowledge of the global budget, including the pathways to and from the reservoir of internal
140 wave energy, is key to fully characterize the impact of internal wave-driven mixing on global-scale

141 ocean dynamics. The estimated energy budget of the open-ocean internal wave field is shown in
142 Figure 3. Energy from three major sources contributes to internal waves: tides, surface winds
143 associated with synoptic and mesoscale atmospheric disturbances, and geostrophic currents. Tidal
144 flow moving water over uneven seafloor topography adds about 1 TW of power to the internal
145 wave field. A resonant response in the surface mixed layer to time-varying wind stress provides an
146 estimated 0.3-1.4 TW of power, part of which fuels the internal wave field. Geostrophic currents
147 flowing over small-scale topographic features, or losing balance, transfer energy to internal waves
148 at estimated global rates of 0.15-0.75 TW and 0.1-0.36 TW, respectively.

149 Once internal waves are generated, they enter the global reservoir of internal wave energy (Fig-
150 ure 3). This reservoir has a remarkably consistent distribution of wavenumbers and frequencies,
151 presumably due to the prevalence of wave-wave interactions in distributing energy across length
152 and time scales [49], which is modeled by the empirically derived Garrett-Munk spectrum [50, 51].
153 Observations reveal a more complex internal wave spectrum with considerable spatio-temporal vari-
154 ability [52, 53], including peaks at the tidal and inertial frequencies that are respectively attributed
155 to generation by tides and time-variable winds, in addition to pronounced deviations near topogra-
156 phy [54] and in shallow water [55, 56]. However, a complete understanding of what sets the energy
157 level and shape of the internal wave spectrum, in particular the ‘continuum’ of the spectrum where
158 there are no peaks, is still an area of active research.

159 Globally, the energy in the internal wave field is either lost through turbulent dissipation or
160 transferred to the background ocean currents. Dissipation can occur close to the waves’ generation
161 sites, or up to thousands of kilometers away, making tracking energy through the system extremely
162 challenging. Along the way, the internal waves are thought to exchange energy with the back-
163 ground current field, adding to the difficulty of closing the global internal wave energy budget and
164 comprehensively mapping internal wave-driven mixing.

6. Tides

165

166 Energy from the tides is a major contributor to the internal wave field energy budget [57],
167 globally converting about 1 TW of energy to open-ocean internal tides [58, 59]. Once internal
168 waves at the tidal frequencies and their harmonics are generated, they travel through the ocean
169 differently depending on their spatial scale; generally the high-mode waves dissipate in the near field
170 (close to the generation site) and low-mode waves dissipate in the far field. The many pathways
171 of internal tides from generation to dissipation yield a complex global geography of internal tide
172 dissipation [60, 61, 62, 63], shown in Figure 4a.

173 **6.1. Generation.** Gravitational attraction of the moon and sun generates the ocean’s barotropic
174 tides [G] [57], which uniformly span the full water column. Barotropic tidal currents dissipate
175 about two thirds of their energy through friction and shear-driven mixing in shelf seas [64] and
176 breaking coastal lee waves [65, 66]. The remainder of barotropic tidal energy is dissipated through
177 the generation of internal (baroclinic) tides [G], resulting from the periodic displacement of density
178 surfaces by barotropic tidal currents pushing stratified fluid along a sloping seafloor [19, 57].

179 The character of the topography plays a primary role in setting the dominant modes of the
180 internal tide: a tall and steep slope (e.g., a continental slope) tends to generate low-mode internal
181 tides, whereas a flatter but corrugated bottom (e.g., an abyssal ridge flank) favours high modes
182 [67, 68] (Figure 4b). A small number of sharp and steep topographic features contribute the
183 majority of the power going into the first few modes [69, 70]. Internal tides with the smallest
184 scales, corresponding to modes $\gtrsim 50$, are mostly generated by “abyssal hills” [71, 72] that have
185 typical widths of several kilometres and heights of a few hundred meters [73]. Generation by abyssal
186 hills has been estimated to amount to about 0.1 TW globally [72, 74], roughly 10% of the total
187 conversion rate from barotropic to baroclinic tides.

188 **6.2. Near-field mixing.** After internal tides are generated, a portion of the energy is dissipated in
189 the near-field, close to the rough topographic features of origin [75, 76, 71]. In particular, direct non-
190 linear breaking and wave-wave interactions may both be responsible for the rapid energy transfer
191 from high-mode internal tides to turbulence in close proximity to topography [77, 78, 79] and in
192 the upper water column [60, 78, 74]. Evidence for this near-field mixing due to internal waves
193 include microstructure observations accumulated over the last 25 years showing that the turbulent
194 dissipation rate is elevated multiple kilometers above or away from irregular topography, and that
195 it often increases with greater proximity to that topography [75, 62]. Additionally, observations
196 and model studies suggest that abyssal hill roughness underpins the bulk of the bottom-enhanced
197 turbulence occurring over ridge flanks of the Pacific, Atlantic and Indian basins [78, 80, 74].

198 The geography of near-field mixing is challenging to model because the fraction of energy dissi-
199 pated in the near field, and its vertical distribution, are a function of numerous factors including the
200 local environment and the modal content of the internal tide. As a consequence of this complexity,
201 in situ observations and theory indicate that the fraction of energy dissipated in the near field may
202 range between 0.1 and 1 [81, 82, 78, 62, 74, 68]. The power input to modes ≥ 4 compares well with
203 depth-integrated dissipation rates measured with microstructure probes, suggesting that modes ≥ 4
204 dissipate mostly near their generation site [68]. These high modes represent an estimated 606 GW,
205 or 49% of the total generation at seafloor depths exceeding 500 m [68]. Parameterizations of the full
206 water column vertical distribution of near-field dissipation [78, 74] are often based on observations
207 from the eastern Brazil Basin. Since the accuracy of these parameterizations on a global scale is
208 largely unknown, observations across different regimes of high-mode internal tide generation [80, 83]
209 will help to develop and improve confidence in parameterizations.

210 **6.3. Propagation and far-field mixing.** The distance that low-mode internal tides travel before
211 dissipating their energy – often in the far field – depends on the mode number of the wave and the

212 oceanic environment along the wave’s path. First-mode internal tides propagating up to several
213 thousands of kilometres can be detected using acoustic tomography and satellite altimetry [84, 85]
214 and are dominated by distinct beams 100-300 km wide [70, 86] (Figure 4c). By contrast, identified
215 mode-2 beams are more numerous but weaker, narrower and an order of magnitude shorter [87].
216 Mode 1 accounts for the bulk of internal tide horizontal energy transport [88], though modes 2-5
217 also contribute substantially [89, 90]; however, the exact fraction of energy transport in each mode
218 depends on a number of environmental factors described below.

219 First, as internal waves propagate, variable bathymetry plays an important role in the transfer
220 of low-mode energy to smaller scales, channeling the energy closer to the scale at which dissipation
221 occurs [91, 92, 63]. When a large-scale wave bounces off short-scale seafloor irregularities, part
222 of its energy is scattered into higher modes [93, 94], leading to bottom-intensified turbulence and
223 dissipation. Larger-scale seamounts or ridges can also cause scattering to higher modes, as well
224 as refraction of incident beams [52, 95, 96]. Beams that ultimately reach continental margins can
225 reflect backward, dissipate or shoal, depending in part on the local topographic slope. Backward
226 reflection dominates if the continental slope is significantly steeper than the wave [97, 98]. If the
227 topographic slope is approximately equal to the wave slope, energy is transferred to very high
228 modes that break into small-scale turbulence along the slope [99, 100, 101]. Gentler continental
229 slopes allow the internal tide to progress into shallow waters; however, as energy concentrates in
230 the vertical, shear increases and direct breaking of the wave is frequent, particularly at the shelf
231 break [102].

232 In addition to interactions with bathymetry, wave-wave interactions may also be significant in
233 attenuating the mode-1 internal tides, and are likely dominant in draining energy from modes \geq
234 2 [28, 103, 38, 63]. The energy transfer is most efficient equatorward of the latitude at which
235 the tidal frequency is twice the inertial frequency—that is, equatorward of 29° for the dominant

236 semidiurnal tidal constituent [29]. Resonant triads transfer energy to smaller vertical wavelengths,
237 and ultimately to dissipation focused in the stratified upper ocean [104, 105, 106].

238 Finally, the propagation and modal content of internal tides can additionally be altered by
239 interactions with the shear, strain and varying stratification present in mesoscale eddies, equatorial
240 jets and other background ocean currents [107, 108, 109, 110, 111, 112]. The interactions can
241 potentially transfer energy to higher modes, leading to dissipation, or transfer energy between
242 low-mode internal tides and the background ocean currents. Additional observational studies of
243 low-mode internal tide energy loss via interactions with background currents are needed, since the
244 significance of such interactions for internal tide-driven mixing is not yet well known.

245 Global estimates of the distribution of mode-1 internal tide energy dissipation suggest that large-
246 scale topographic obstacles cause the bulk of that dissipation [91, 63]. Using Lagrangian tracking of
247 energy beams and parameterized energy sinks, it has been estimated that wave-wave interactions
248 explain about 25% of mode-1 dissipation, but 65-80% of the overall modes 1-5 dissipation [63].
249 Hence, despite major topographic features hosting the bulk of mode-1 dissipation, much of the
250 observed open-ocean internal tide dissipation may originate from the far-field dissipation of modes
251 2-5. Scattering by abyssal hills could be responsible for about 10% of the dissipation of the first
252 five modes [63]. However, additional constraints on attenuation rates of low-mode internal tides by
253 wave-wave interactions, and improved understanding of interactions with rough topography and
254 background currents, are called for to narrow down uncertainties in these exploratory estimates.

255

7. Wind

256 Time-variable winds, often associated with passing storms, can provide power for near-inertial
257 waves [G] (internal waves near the inertial frequency) to grow [113]. As storm activity increases in
258 the winter, so does the energy in the near-inertial wave field and associated mixing rates, suggesting
259 that winds are a key driver of the seasonal variability of internal wave-driven mixing in the ocean

260 [114, 115]. However, the main mechanisms leading near-inertial waves to dissipate their energy are
261 not yet well constrained, leaving ample opportunity for future work.

262 The following divides the lifecycle of near-inertial waves into a generation phase, namely how
263 near-inertial energy injected into the mixed layer by the wind is transferred to the ocean interior,
264 followed by an internal wave propagation and mixing phase. Note that this division is distinct
265 from conceptually partitioning the wave’s lifecycle into an active wind-forcing phase, followed by the
266 ocean’s response after the forcing ends—a framework employed by some studies of isolated events
267 [116].

268 **7.1. Generation.** Time-varying wind stress on the ocean surface due to synoptic events, such as a
269 passing mid-latitude storm [116] or cyclone [117, 118, 119], can generate a resonant response in the
270 mixed layer of water oscillating horizontally at a frequency close to inertial. The signature of near-
271 inertial oscillations can be observed in the circles traced by surface drifters distributed beneath a
272 storm [116]. One way that inertial oscillations decay is through energy dissipation by shear-driven
273 turbulence close to the mixed layer base [120, 121]; however, the importance of this mechanism is
274 poorly known. The second, potentially more important, mechanism is downward energy radiation
275 into the stratified interior ocean. Specifically, internal waves are radiated downward when horizontal
276 variability in the magnitude of near-inertial velocities creates divergences and convergences within
277 the mixed layer, generating pressure gradients that allow water to locally rise and fall at the inertial
278 frequency, thereby radiating energy [122] (Figure 5).

279 The portion of near-inertial energy escaping the mixed layer as internal waves is not well con-
280 strained. Combining two lower-bound observational estimates of the fraction of energy propagating
281 away as low-mode [123] and high-mode [124] waves suggests that a minimum of 27-53% of the en-
282 ergy input into near-inertial oscillations radiates away as internal waves. Roughly consistent with
283 this observation, seasonal cycles in the mixed-layer and deep-ocean near-inertial kinetic energy are

284 all similar in magnitude [114, 125]. However, global modeling studies find that a smaller fraction of
285 the wind work on near-inertial motions radiates downward, with estimates of 11-30% leaving the
286 vicinity of the mixed layer [126, 127, 128]. Modeling studies with high spatio-temporal resolution
287 suggest that resolving the interactions between the mesoscale eddy field and inertial oscillations
288 may be important [129]; however, more work is needed to improve and reconcile observational and
289 model-based estimates of downward near-inertial energy propagation.

290 Advancing our understanding of how the growth and decay of near-inertial oscillations can be
291 modified by the background oceanic environment may help constrain the magnitude of energy
292 leaving the mixed layer. For example, spatial variations in the Coriolis frequency may reduce the
293 internal wave length scales [116], increasing the rate at which near-inertial energy drains from the
294 mixed layer. Additionally, as near-inertial oscillations grow, energy transfer can occur with the
295 background flow due to strong horizontal convergence [130], and horizontal strain [131] at a rate
296 modulated by anticyclonic rotation [132, 131]. During the decay of near-inertial oscillations, strong
297 gradients in vorticity can increase the radiation of near-inertial energy from the mixed layer [133],
298 especially at sharp gradients in the background currents [134, 133, 135].

299 Global studies commonly target a specific phase of the near-inertial wave generation process:
300 the energy flux from winds to near-inertial oscillations. Estimates of the power available for near-
301 inertial wave generation are often made using atmospheric reanalysis-derived winds to force general
302 circulation models [136, 137], and 1-d slab models where the mixed layer is set to a fixed depth and
303 energy radiates away at an assigned timescale [113, 116, 138, 139, 140]. The slab model produces
304 estimates that agree well with observations, with caveats [140, 141]. Products with relatively high
305 temporal and spatial resolutions (reanalysis winds available at least every 4 hours, and satellite
306 altimetric data sets with 1 degree horizontal resolution or finer) yield 0.9-1.4 TW of global power
307 input from the winds [142, 137], while estimates from coarser temporal and/or spatial resolution
308 winds suggest 0.3-1 TW [143, 142, 139, 136, 137]. Both of these estimates are consistent with the

309 first drifter-based estimate that finds a lower bound of 0.3 TW [144]; however, more observational
310 work is needed to reduce the large uncertainties in all estimates.

311 **7.2. Local and Far field Mixing.** Distinct high-mode near-inertial waves can be observed as
312 bands of alternating shear at vertical scales of metres to hundreds of metres. In the North Pacific,
313 observations reveal that high-mode near-inertial waves can attain vertical group velocities of 7-
314 23 m/day [124] and horizontal scales of 10s to 100s of kilometers [145]. Observational estimates
315 indicate that the fraction of wind work on mixed layer oscillations that propagates away as high-
316 mode near-inertial waves may range between 12-33% (reaching 800 m)[124], or 2-33% (reaching 100
317 m)[146]. Modelling studies provide the slightly smaller estimate that 10% [127] of the wind work
318 on the mixed layer reaches 230 m as high-mode internal waves.

319 In addition to high-mode internal waves, a large fraction of near-inertial energy is thought to
320 radiate away as low modes, with estimates ranging from 15-20% of the energy input into mixed
321 layer oscillations [123], to 33-45% of the near-inertial wave energy in the thermocline (modes 1-2)
322 [116]. Since the Coriolis frequency decreases towards the equator and sets the internal wave low-
323 frequency limit, near-inertial waves are typically constrained to propagate equatorward [147, 123]
324 except in strongly sheared background flows [148]. As the low modes propagate, they are subject
325 to wave-wave interactions, including parametric subharmonic instability [149, 150], that can reduce
326 their length scales and lead to turbulent mixing.

327 Near-inertial wave activity is elevated beneath mid-latitude storm tracks, with a seasonal cycle
328 that peaks in the winter months from the surface to the seafloor [114, 151] (Figure 5 a-b); however,
329 the mechanisms underpinning such a deep seasonal cycle are not well understood. The stronger
330 near-inertial wave activity during the winter months is correlated with an enhancement of inferred
331 diapycnal mixing [48, 152, 115] to at least a depth of 2 km (Figure 5 c-d). Future work linking
332 direct observations of mixing using microstructure methods to the seasonal cycle in near-inertial

333 kinetic energy would be valuable to corroborate the implication of near-inertial waves in driving
334 seasonality in mixing.

335 The mesoscale flow field likely shapes the rate of near-inertial propagation and spatial distri-
336 bution of the energy dissipation, in addition to influencing the generation processes described in
337 the previous subsection. Modelling and theory suggest that the mesoscale vorticity can reduce
338 the horizontal scales of the waves and funnel near-inertial energy into regions of anticyclonic vor-
339 ticity [153, 154, 155, 156, 129]. Additionally, a positive strain rate in the mesoscale current field
340 can substantially alter the length scales and propagation velocities of internal waves [32, 109, 53].
341 Finally, internal waves can encounter critical layers along steeply sloping isopycnals, triggering
342 energy dissipation [157, 153, 158, 159]. Observations support these general ideas, finding altered
343 internal waves and elevated dissipation rates at the boundaries of individual mesoscale eddies
344 [160, 161, 162, 163, 164], and relatively large inferred mixing in response to increased wind activity
345 in the presence of an energetic mesoscale eddy field [115].

346 8. Geostrophic Currents

347 Winds provide about 1 TW of power to the geostrophic current field in the ocean [165, 166].
348 A portion of the energy in ocean currents is then transferred to the internal wave field through
349 interactions with topographic features, or by direct generation of internal waves. However, it
350 has been suggested that the bulk of the energy in the geostrophic current field is not dissipated
351 through internal wave processes, but by a combination of bottom friction [167, 168], hydraulic
352 effects downstream of topography [169], and suppression by wind work [8, 170].

353 **8.1. Quasi-steady lee wave generation at topographic features.** When steady or eddying
354 abyssal flows impinge on small-scale topographic features, they can generate internal waves, often
355 called lee waves [G] [19]. Internal lee waves have frequencies and length scales set by the velocity
356 of the currents and length scales of the bathymetry. Estimates made using linear wave theory [19]

357 of the total global energy transfer rate from geostrophic currents into internal lee waves range from
358 0.15 to 0.75 TW [171, 172, 173, 174, 175], with a major contribution from the Antarctic Circumpolar
359 Current (ACC) region. These estimates' large range arises from uncertainties in ocean stratification,
360 bathymetric products and, principally, the representation of near-bottom current speeds in global
361 circulation models [173, 176].

362 Once generated, lee waves can travel upwards if the frequency in the wave's reference frame is
363 between f and N . In a steady current, propagating lee waves appear stationary in the ground
364 reference frame, but can shift upstream or downstream if the current varies in time or nonlinear
365 interactions are present [19, 177]. Most of the evidence for lee wave activity in the ACC has been
366 provided by indirect measurements of elevated upward-propagating internal wave energy in the
367 deepest 1-2 km of the water column [178, 179, 180]; however, an unambiguous observation was
368 made of the waves themselves [181] (Figure 6a). Observations in the western boundaries of mid-
369 latitude ocean basins also show evidence for the generation and propagation of internal lee waves
370 there [182]. Lee wave radiation is highly intermittent due to changes in the intensity and position
371 of the background flow, resulting in temporal variability of the lee wave field on time scales up to
372 decadal [183, 184, 185].

373 Lee waves' energy is dissipated as the waves encounter critical layers, or as the energy is trans-
374 ferred to other waves via wave-wave interactions or reabsorbed into the background current field
375 [186]. Observations of elevated turbulence attributed to lee waves include studies in the ACC
376 [187, 188, 178, 179, 180], abyssal passages [189], and canyons [190]. Estimates of the amount of
377 radiated lee wave energy that is dissipated within 1 km of the bottom range from up to 50% using
378 2-d models [191] to 2-30% using observations [178, 179]. The discrepancy between these estimates
379 highlights that lee waves do not play as important a role in the internal wave global energy bud-
380 get as early modeling studies suggested. Additional complexity, such as including 3-d flow effects,

381 is necessary to model lee wave generation, propagation, and dissipation more accurately than in
382 current modelling efforts [47, 174, 179, 192, 169, 177, 186].

383 **8.2. Internal wave generation from geostrophic currents.** The generation of internal waves
384 directly from the geostrophic current field may contribute to sustaining turbulent dissipation and
385 mixing, although the contribution may be relatively small. Modelling results demonstrate that
386 internal waves near the inertial frequency can be generated through resonance with the rapidly
387 varying components of background currents [193, 194, 195, 196] and, more specifically, during
388 intense straining of small-scale fronts by the larger-scale currents [197, 198, 199]. Additionally, an
389 actively unstable front might radiate internal waves with a larger range of frequencies [200, 201].
390 Finally, geostrophic currents can also transfer energy to existing near-inertial waves, providing an
391 additional energy pathway [202, 203]. Estimates of the global energy flux from geostrophic currents
392 to internal waves range between 0.1 and 0.36 TW [8, 204, 198]. However, only limited observations
393 of this internal wave generation pathway exist [205, 198], so the prevalence of these processes is
394 still unclear.

395 The eventual fate of the internal waves drawing energy from geostrophic flows is either turbulent
396 dissipation (Figure 6b) or re-absorption into the background current field. If a substantial portion
397 of the energy from these internal waves dissipates via wave breaking, then the waves may be
398 a significant energy sink for the mesoscale eddy field [206]. However, modelling results suggest
399 that only around 15% [198] or 30% [207] of the energy is dissipated through turbulence, with
400 the remainder returning to the background current field. The low fraction of dissipated energy
401 indicates that the internal waves generated from ocean currents may be an important mechanism
402 for redistributing energy, but contribute only modestly to the global internal wave and mesoscale
403 eddy kinetic energy budgets.

405 All the processes governing the generation, propagation, and dissipation of internal waves deriv-
406 ing their energy from tides, winds and geostrophic currents conspire to shape the global distribution
407 of the turbulent dissipation rate and diapycnal diffusivity as observed using microstructure [62] and
408 finestructure [60, 61, 9, 115] measurements (Figure 7a). The intensity of the dissipation rate and
409 diffusivity both range over three orders of magnitude across the globe, so that the bulk of the
410 values span 10^{-11} - 10^{-8} [W/kg] and 10^{-6} - 10^{-3} [m^2/s], respectively [60, 61, 62]. When the bottom
411 topography is rough, the dissipation rate is often elevated by an order of magnitude or more from
412 the seafloor to near the surface, due to near-field dissipation of internal tides or lee waves as well
413 as mixing from topographic scattering of remotely generated internal waves [60, 61, 106]. Regions
414 with strong sources of tidal and wind energy are also associated with elevated dissipation rates,
415 indicating that near-field dissipation plays an important role in shaping the global geography of
416 mixing [115, 68]. For example, mixing is elevated above the Hawaiian Ridge, Southwest Indian
417 Ridge and Mid-Atlantic Ridge due to tidal generation and scattering [82, 75, 63]. In the South-
418 ern Ocean around the Kerguelen Plateau and Macquarie Ridge, lee waves and tides may both
419 contribute [178, 174, 92].

420 As explained in the following, mixing from internal waves contributes to sustaining the deep
421 ocean's meridional overturning circulation, and importantly influences the broader global climate
422 system, in addition to impacting the oxygen distribution [12], the delivery of nutrients to the ocean's
423 surface layers [14], and primary production [12].

424 **9.1. Global Overturning Circulation.** The cold, dense water that sinks to the ocean abyss
425 at high latitudes must eventually rise, returning to the ocean surface and thereby closing the
426 Meridional Overturning Circulation (MOC). The simplified model of the MOC has two major

427 branches. One of the branches transports deep water southward, and is primarily driven by wind-
428 induced upwelling in the Southern Ocean [208], although in models its strength is sensitive to
429 changes in mixing [209, 210, 211, 129]. The second branch, in turn, transports abyssal water
430 northward and upward [4], and is thought to be largely driven by internal wave mixing [3, 62, 5, 6],
431 with additional contributions from geothermal heating along the seafloor [212, 213] and mixing
432 along the deep western boundaries [214] and within constrictive passages [215].

433 In the northward branch of the abyssal MOC, turbulence from breaking internal waves transfers
434 buoyancy downward, progressively transforming the dense bottom water into lighter water. This
435 lightening enables new inflowing water to intrude below, such that the transformed water rises
436 above the new water, creating the upward branch of the abyssal MOC. The strength of this branch
437 has been estimated to be 20-30 Sverdrups (Sv; $1 \text{ Sv} \equiv 10^6 \text{ m}^3\text{s}^{-1}$) [216, 217, 4]. Internal tides
438 are thought to drive a substantial portion of the abyssal upwelling, with estimates including both
439 near-field and far-field mixing that range between the entirety of the abyssal MOC transport to 7
440 Sv [218, 5], or 5 Sv with a spatially variable mixing efficiency [219]. Lee waves contribute a smaller
441 portion of the abyssal upwelling, with estimates ranging between 2-3 Sv [220, 5]. It is not known
442 if near-inertial waves play a significant role in driving the abyssal MOC. Both the horizontal and
443 vertical distributions of mixing alter the magnitude and vertical structure of the MOC in models
444 [221, 222, 218, 209, 223, 220, 210], an example of which is shown in Figure 7b, indicating that the
445 global spatial variability (Figure 7 a) is important for setting the observed properties of the MOC.

446 **9.2. Climate.** The broader climate system is sensitive to the distribution and magnitude of internal
447 wave-driven mixing in the ocean, beyond the role of mixing in driving the MOC as discussed in
448 the previous subsection. Since diffusivity from internal waves cannot be explicitly captured by
449 global models, parameterizations are currently being developed to include the effects of the spatio-
450 temporally varying diffusivity [21]. To explore how sensitive the ocean and atmosphere are to

451 mixing from breaking internal waves, climate models are run with a range of parameterizations
452 designed to represent mixing from the tides [106, 210, 224, 225], winds [106, 226, 225] and lee waves
453 [220, 227], in addition to changing the magnitude of the model-prescribed background diffusivity
454 [211]. These studies report that even small perturbations in the magnitude or distribution of the
455 diffusivity in global models can lead to substantial changes in the temperature, circulation, and
456 fluxes in the atmosphere and ocean. However, both the magnitude and the sign of these changes
457 vary between studies due to the range of mixing parameterizations and the details of each model,
458 thus the following focuses on the broad trends across all studies.

459 Altering the diffusivity changes the vertical profiles and horizontal distribution of temperature
460 and salinity throughout the ocean, and therefore the density and stratification [226, 220, 227, 210,
461 224, 211, 225]. The ocean’s meridional heat transport is also sensitive to changing background
462 diffusivity and to the spatial distribution of mixing from internal tides [210, 211], but not to pa-
463 rameterized mixing induced by near-inertial waves in one study that underestimates the magnitude
464 of mixing from the wind [226]. Changes in the properties and circulation of the ocean interior
465 lead to variations in the sea surface temperature [226, 210, 211, 225], mixed layer depth [226, 224],
466 and air-sea fluxes [129, 211]. Perturbing interior diffusivity also has repercussions above the sea
467 surface, including sea ice extent and concentration [226, 224, 211], air temperature, atmospheric
468 circulation, and precipitation [226, 224, 211, 225]. For example, one study added diffusivity from
469 near-inertial internal waves and found notable changes in the sea ice extent and surface heat flux
470 (Figure 7c)[226]. The substantial sensitivity of both the ocean and the atmosphere to internal
471 wave mixing indicates that including its effects in climate-scale models is important for a realistic
472 representation of the climate system.

473 Beyond these widespread climatic impacts, internal wave mixing has been shown to exert a pro-
474 found influence on regional and global climate via its localised effects on several important elements
475 of the global ocean circulation. For example, the vertical density structure in the Indonesian Seas

476 is sensitive to the representation of tidal mixing in models—with implications for a range of aspects
477 of (sub-)tropical Indo-Pacific climate including volume transport of the Indonesian Throughflow,
478 ocean heat uptake, and rainfall [228, 229, 230]. In the equatorial Pacific, parameterizing internal
479 wave mixing in the thermocline yields changes in the equatorial upwelling, sea surface tempera-
480 ture, and wind patterns [226, 225]. However, only representing mixing from tides or lee waves has a
481 negligible effect [220, 210], suggesting that including more processes than current tide and lee wave
482 parameterizations represent may be necessary to accurately model the equatorial Pacific. Finally,
483 the latitudinal distribution of deep mixing from lee waves and tides has been argued to alter the
484 ACC transport, the depth of the ocean thermocline and, by extension, many important features of
485 global climate [231, 232, 220]. As the operation of internal wave mixing in other pivotal elements of
486 the global ocean circulation is further unravelled, it is likely that more climatic impacts of localised
487 mixing will emerge.

488 10. SUMMARY AND FUTURE DIRECTIONS

489 Global and regional patterns of internal wave-driven turbulent mixing are controlled by the com-
490 plex and convoluted processes of internal wave generation, propagation, interaction and dissipation.
491 Internal waves act as a conduit, eventually funneling energy from tides, winds, and currents into
492 turbulence, leading to both energy dissipation and mixing. In turn, the mixing plays a role in
493 driving the meridional overturning circulation and aids in setting many characteristics of the global
494 climate. While much progress has been made recently in understanding significant elements of
495 all stages of the internal wave lifecycle, several fundamental knowledge gaps remain. Here, we
496 synthesize these gaps into three broad priority challenges, which we encourage the oceanographic
497 community to address in coming years.

498 The first challenge entails advancing our understanding of the processes that transfer energy
499 within the internal wave field, and which ultimately lead to dissipation and mixing. As discussed

500 here, investigations have improved constraints on the wave field’s energy sources, and the magnitude
501 and placement of wave energy dissipation. However, the physics of how the energy is transferred
502 across length scales and frequencies along the pathway to dissipation is poorly understood. In
503 particular, we do not know why the observed internal wave spectrum varies only modestly in shape
504 across the global ocean [53]. Important likely candidates include wave-wave interactions [29, 26],
505 topographic scattering and reflection [93], and interactions with the background current field [233].
506 Studies focused on these individual energy transfer processes, and on how they combine to form the
507 observed internal wave spectrum, would be valuable. For example, recent investigations suggest
508 that parametric subharmonic instability, the very efficient type of wave-wave interaction, is not
509 sufficient to explain the majority of the down-scale internal wave energy transfer [29], indicating
510 that other wave-wave interactions [26] or wave-wave interactions in the context of geostrophic
511 currents [83] may be important in shaping the spectrum. Additional theoretical and numerical
512 work constraining attenuation due to wave-wave interactions using an internal wave spectrum close
513 to that observed in the ocean is especially needed [38, 29].

514 The second challenge concerns unravelling how internal waves interact with other types of ocean
515 currents, and how these interactions shape the distribution of mixing in the ocean. Interactions
516 between internal waves and currents deserve special consideration, since among the energy exchange
517 processes depicted schematically in Figure 3 and discussed in challenge one, they have the largest
518 uncertainties. The mildest form of this interaction is a gradual shift in the wave phase as waves
519 travel through a current field; for example, this de-phasing may occur as low-mode internal tides
520 propagate through a variable mesoscale flow. De-phasing of low modes renders them invisible to
521 detection by satellite altimetry, increasing the uncertainty in estimates of low-mode attenuation and
522 subsequent energy dissipation [111, 234, 235]. An improved understanding of the weak modulation
523 of internal waves by background currents is needed, especially with a view to constraining low-mode
524 internal tide attenuation and dissipation in global models [210, 63].

525 Moderate interactions involve the impact of spatio-temporal variability of background currents,
526 which present a variable medium for internal waves to exist in and propagate through. Background
527 current flow and vorticity affect internal wave generation by, for example, altering the rate of energy
528 transfer to both internal lee waves and wind-driven near-inertial internal waves. Then, as waves
529 propagate, structure in the background current shear, strain or stratification can lead to significant
530 wave refraction, reflection or, in extreme cases, wave breaking as propagation slows down to a
531 halt in critical layers or sharp fronts. Theoretical, modelling and observational studies are needed
532 to understand the influence of these moderate interactions on the generation, propagation, and
533 dissipation of internal waves, in addition to their prevalence in the ocean and cumulative impact
534 on energy pathways.

535 The strongest form of interaction involves substantial two-way energy exchanges between inter-
536 nal waves and geostrophic flows. For example, for internal lee waves, accurate understanding of
537 refraction in sheared background flows like the ACC is key to predict where and how the waves will
538 deposit their momentum to accelerate or decelerate the background flow [236]. Two-way energy
539 exchanges between internal waves and background flows are also likely to be important where the
540 spatio-temporal scales of both classes of flows overlap, for example in submesoscale (0.1-10 km
541 scales) flows on the edges of mesoscale eddies, or near-inertial waves with slow group velocities
542 and large horizontal wavelengths. The small-scale and quickly varying energy exchanges in these
543 settings are extremely difficult to observe, calling for the development of new, multi-platform mea-
544 surement approaches and numerical simulations of increased complexity. We anticipate that a step
545 change in understanding of how the ocean's mesoscale eddy field loses its energy to internal waves
546 and turbulence will result in major improvements in the realism of climate-scale ocean models,
547 some of whose key features (for example, deep-ocean MOC, ACC transport, stratification) are now
548 understood to depend on the eddy-internal wave energy transfer [206].

549 Building on these challenges, the overarching (and arguably most daunting) task is to reformulate
550 internal wave-driven mixing as a fully interactive component of ocean circulation and the climate
551 system [106], rather than the essentially passive and unchanging diffusivity field as which wave
552 mixing has been traditionally viewed. More work is needed to further develop parameterizations
553 of mixing and quantify their effects on global ocean circulation and climate. For example, more
554 studies are needed that include parameterized mixing from near-inertial waves and explore the
555 impact of time-varying mixing so that feedbacks on the climate system are represented. To drive
556 this transformation, we require new ways to measure internal wave mixing over the annual or longer
557 time scales that are most climatically relevant. In addition, the next generation of physically robust
558 representations of the key wave mixing processes will need to be incorporated into climate-scale
559 ocean models. The spark for this shift in view has been lit by a number of recent studies mentioned
560 in this review, but much work remains to be done for the shift to be realized.

561 11. GLOSSARY OF KEY TERMS

562 **Internal wave orthogonal modes:** Theoretical framework used to describe the vertical struc-
563 ture of internal waves, where low-mode internal waves have larger vertical scales and high-mode
564 internal waves have smaller vertical scales.

565 **Buoyancy frequency (N):** The oscillation frequency of a vertically displaced water parcel,
566 which scales with the local vertical stratification gradient.

567 **Coriolis/inertial frequency (f):** The oscillation frequency of a horizontally displaced water
568 parcel influenced solely by the earth's rotation and defined by $2\Omega \sin\phi$, where Ω is the angular
569 velocity of the earth and ϕ is the latitude.

570 **Turbulent kinetic energy dissipation rate (ϵ):** Rate of energy dissipation due to viscosity
571 with units $W\ kg^{-1}$.

572 **Diapycnal diffusivity (K):** Diffusivity across density surfaces with units m^2s^{-1} .

573 **Barotropic tides:** Nearly full-depth periodic rise and fall of ocean water due to the gravitational
574 attraction of the moon and sun.

575 **Baroclinic/internal tides:** Depth-varying oscillations at tidal frequencies arising from barotropic
576 tides impinging on topographic features.

577 **Near-Inertial internal waves:** Internal waves at or near the Coriolis/inertial frequency, often
578 but not always generated by the wind.

579 **Lee waves:** Internal waves often generated by deep geostrophic flow encountering topographic
580 features.

581 12. ACKNOWLEDGEMENTS

582 This work was supported by the National Aeronautics and Space Administration award 80NSSC19K1116
583 and National Science Foundation award OCE–1923558. ACNG acknowledges the support of the
584 Royal Society and Wolfson Foundation.

585 13. AUTHORSHIP

586 CW led the design and writing of the review. CL, ANG, JK, JM, and KS all contributed to the
587 writing.

588 14. COMPETING INTERESTS

589 The authors declare no competing interests.

590 REFERENCES

- 591 [1] Fer, I., Voet, G., Seim, K. S., Rudels, B. & Latarius, K. Intense mixing of the Faroe Bank Channel overflow.
592 *Geophys. Res. Lett.* **37** (2010).
- 593 [2] D’Asaro, E. A. Turbulence in the upper-ocean mixed layer. *Annu. Rev. Mar. Sci.* **6**, 101–115 (2014).
- 594 [3] Munk, W. & Wunsch, C. Abyssal recipes II: energetics of tidal and wind mixing. *Deep-Sea Res. I* **45**, 1977–2010
595 (1998).

- 596 [4] Talley, L. D. Closure of the global overturning circulation through the Indian, Pacific, and Southern Oceans:
597 Schematics and transports. *Oceanogr.* **26**, 80–97 (2013).
- 598 [5] de Lavergne, C., Madec, G., Le Sommer, J., Nurser, A. G. & Naveira Garabato, A. C. On the consumption of
599 Antarctic Bottom Water in the abyssal ocean. *J. Phys. Oceanogr.* **46**, 635–661 (2016).
- 600 [6] Kunze, E. The internal-wave-driven meridional overturning circulation. *J. Phys. Oceanogr.* **47**, 2673–2689
601 (2017).
- 602 [7] Wunsch, C. & Ferrari, R. Vertical mixing, energy, and the general circulation of the oceans. *Annu. Rev. Fluid*
603 *Mech.* **36**, 281–314 (2004).
- 604 [8] Ferrari, R. & Wunsch, C. Ocean Circulation Kinetic Energy: Reservoirs, Sources, and Sinks. *Ann. Rev. Fluid*
605 *Mech.* **41**, 253–282 (2009).
- 606 [9] Kunze, E. Internal-Wave-Driven Mixing: Global Geography and Budgets. *J. Phys. Oceanogr.* **47**, 1325–1345
607 (2017).
- 608 [10] Anderson, L. A. & Sarmiento, J. L. Redfield ratios of remineralization determined by nutrient data analysis.
609 *Global Biogeochem. Cycles* **8**, 65–80 (1994).
- 610 [11] Sarmiento, J. L., Gruber, N., Brzezinski, M. & Dunne, J. High-latitude controls of thermocline nutrients and
611 low latitude biological productivity. *Nature* **427**, 56 (2004).
- 612 [12] Friedrich, T., Timmermann, A., Decloedt, T., Luther, D. & Mouchet, A. The effect of topography-enhanced
613 diapycnal mixing on ocean and atmospheric circulation and marine biogeochemistry. *Ocean Modelling* **39**,
614 262–274 (2011).
- 615 [13] Deutsch, C. & Weber, T. Nutrient ratios as a tracer and driver of ocean biogeochemistry. *Annu. Rev. Mar. Sci.*
616 **4**, 113–141 (2012).
- 617 [14] Tuerena, R. E. *et al.* Internal tides drive nutrient fluxes into the deep chlorophyll maximum over mid-ocean
618 ridges. *Global Biogeochem. Cycles* (2019).
- 619 [15] Sharples, J. Internal tides drive nutrient fluxes into the deep chlorophyll maximum over mid-ocean ridges. *Global*
620 *Biogeochem. Cycles* (2019).
- 621 [16] Phillips, O. M. *The dynamics of the upper ocean* (CUP Archive, 1966).
- 622 [17] Woods, J. Wave-induced shear instability in the summer thermocline. *J. Fluid Mech.* **32**, 791–800 (1968).
- 623 [18] Garrett, C. & Munk, W. Internal waves in the ocean. *Annu. Rev. Fluid Mech.* **11**, 339–369 (1979).
- 624 [19] Bell, T. Topographically generated internal waves in the open ocean. *J. Geophys. Res.* **80**, 320–327 (1975).

- 625 [20] Munk, W. H. Abyssal recipes. In *Deep-Sea Res. Oceanogr. Abstr.*, vol. 13, 707–730 (Elsevier, 1966).
- 626 [21] MacKinnon, Z., Jennifer A Zhao *et al.* Climate Process Team on Internal-Wave Driven Ocean Mixing. *Bull.*
627 *Am. Meteorol. Soc.* **98**, 2429–2454 (2017).
- 628 [22] Alford, M. H., MacKinnon, J. A., Simmons, H. L. & Nash, J. D. Near-inertial internal gravity waves in the
629 ocean. *Annu. Rev. Mar. Sci.* **8**, 95–123 (2016).
- 630 [23] Gill, A. E. *Atmosphere—ocean dynamics* (Elsevier, 2016).
- 631 [24] Olbers, D. J. Nonlinear energy transfer and the energy balance of the internal wave field in the deep ocean. *J.*
632 *Fluid Mech.* **74**, 375–399 (1976).
- 633 [25] Lvov, Y. V., Polzin, K. L. & Yokoyama, N. Resonant and near-resonant internal wave interactions. *J. Phys.*
634 *Oceanogr.* **42**, 669–691 (2012).
- 635 [26] Eden, C., Pollmann, F. & Olbers, D. Numerical evaluation of energy transfers in internal gravity wave spectra
636 of the ocean. *J. Phys. Oceanogr.* **49**, 737–749 (2019).
- 637 [27] Hibiya, T., Nagasawa, M. & Niwa, Y. Nonlinear energy transfer within the oceanic internal wave spectrum at
638 mid and high latitudes. *J. Geophys. Res. Oceans: Oceans* **107**, 28–1 (2002).
- 639 [28] MacKinnon, J. A. *et al.* Parametric subharmonic instability of the internal tide at 29 N. *J. Phys. Oceanogr.*
640 **43**, 17–28 (2013).
- 641 [29] Olbers, D., Pollmann, F. & Eden, C. On PSI interactions in internal gravity wave fields and the decay of
642 baroclinic tides. *J. Phys. Oceanogr.* (2020).
- 643 [30] Jones, W. L. Ray tracing for internal gravity waves. *J. Geophys. Res.* **74**, 2028–2033 (1969).
- 644 [31] Staquet, C. & Sommeria, J. Internal gravity waves: from instabilities to turbulence. *Annu. Rev. Fluid Mech.*
645 **34**, 559–593 (2002).
- 646 [32] Bühler, O. & McIntyre, M. E. Wave capture and wave–vortex duality. *J. Fluid Mech.* **534**, 67–95 (2005).
- 647 [33] Thorpe, S. Models of energy loss from internal waves breaking in the ocean. *J. Fluid Mech.* **836**, 72–116 (2018).
- 648 [34] van Haren, H. Instability observations associated with wave breaking in the stable-stratified deep-ocean. *PHYS-*
649 *ICA D* **292**, 62–69 (2015).
- 650 [35] Gregg, M. C., Seim, H. E. & Percival, D. B. Statistics of shear and turbulent dissipation profiles in random
651 internal wave-fields. *J. Phys. Oceanogr.* **23**, 1777–1799 (1993).
- 652 [36] Alford, M. H. & Pinkel, R. Observations of overturning in the thermocline: The context of ocean mixing. *J.*
653 *Phys. Oceanogr.* **30**, 805–832 (2000).

- 654 [37] Olbers, D. J. Models of the oceanic internal wave field. *Reviews of Geophysics* **21**, 1567–1606 (1983).
- 655 [38] Onuki, Y. & Hibiya, T. Decay rates of internal tides estimated by an improved wave–wave interaction analysis.
656 *J. Phys. Oceanogr.* **48**, 2689–2701 (2018).
- 657 [39] Osborn, T. R. Estimates of the local-rate of vertical diffusion from dissipation measurements. *J. Phys. Oceanogr.*
658 **10**, 83–89 (1980).
- 659 [40] Gregg, M., D’Asaro, E., Riley, J. & Kunze, E. Mixing efficiency in the ocean. *Annu. Rev. Mar. Sci.* **10**, 443–473
660 (2018).
- 661 [41] Oakey, N. Determination of the rate of dissipation of turbulent energy from simultaneous temperature and
662 velocity shear microstructure measurements. *J. Phys. Oceanogr.* **12**, 256–271 (1982).
- 663 [42] Gregg, M. Uncertainties and limitations in measuring ε and χ t. *J. Atmos. Ocean. Technol. Annu. Rev. Fluid*
664 *Mech.* **16**, 1483–1490 (1999).
- 665 [43] Henyey, F. S., Wright, J. & Flatte, S. M. Energy and action flow through the internal wave field - an eikonal
666 approach. *J. Geophys. Res.-Oceans* **91**, 8487–8495 (1986).
- 667 [44] Gregg, M. C. Scaling turbulent dissipation in the thermocline. *J. Geophys. Res.-Oceans* **94**, 9686–9698 (1989).
- 668 [45] Polzin, K. L., Toole, J. M. & Schmitt, R. W. Finescale parameterizations of turbulent dissipation. *J. Phys.*
669 *Oceanogr.* **25**, 306–328 (1995).
- 670 [46] Polzin, K. L., Naveira Garabato, A. C., Huussen, T. N., Sloyan, B. M. & Waterman, S. N. Finescale parame-
671 terizations of turbulent dissipation. *J. Geophys. Res.-Oceans* **119** (2014).
- 672 [47] Waterman, S., Polzin, K. L., Naveira Garabato, A. C., Sheen, K. L. & Forryan, A. Suppression of internal wave
673 breaking in the Antarctic Circumpolar Current near topography. *J. Phys. Oceanogr.* **44** (2014).
- 674 [48] Whalen, C. B., MacKinnon, J. A., Talley, L. D. & Waterhouse, A. F. Estimating the mean diapycnal mixing
675 using a finescale strain parameterization. *J. Phys. Oceanogr.* **45**, 1174–1188 (2015).
- 676 [49] McComas, C. H. & Müller, P. The dynamic balance of internal waves. *J. Phys. Oceanogr.* **11**, 970–986 (1981).
- 677 [50] Garrett, C. & Munk, W. Space-time scales of internal waves - progress report. *J. Geophys. Res.* **80**, 291–297
678 (1975).
- 679 [51] Munk, W. Internal waves and small-scale processes, Evolution of Physical Oceanography BA Warren, C. Wun-
680 sch, 264–291 (1981).
- 681 [52] Müller, P. & Liu, X. Scattering of internal waves at finite topography in two dimensions. Part I: Theory and
682 case studies. *J. Phys. Oceanogr.* **30**, 532–549 (2000).

- 683 [53] Polzin, K. L. & Lvov, Y. V. Toward regional characterizations of the oceanic internal wavefield. *Rev. Geophys.*
684 **49** (2011).
- 685 [54] Lien, R.-C., Tang, T., Chang, M. & d’Asaro, E. Energy of nonlinear internal waves in the South China Sea.
686 *Geophys. Res. Lett.* **32** (2005).
- 687 [55] Levine, M. D. A modification of the garrett–munk internal wave spectrum. *J. Phys. Oceanogr.* **32**, 3166–3181
688 (2002).
- 689 [56] MacKinnon, J. & Gregg, M. Shear and baroclinic energy flux on the summer new england shelf. *J. Phys.*
690 *Oceanogr.* **33**, 1462–1475 (2003).
- 691 [57] Garrett, C. & Kunze, E. Internal tide generation in the deep ocean. *Annu. Rev. Fluid Mech.* **39**, 57–87 (2007).
- 692 [58] Egbert, G. & Ray, R. Significant dissipation of tidal energy in the deep ocean inferred from satellite altimeter
693 data. *Nature* **405**, 775 (2000).
- 694 [59] Nycander, J. Generation of internal waves in the deep ocean by tides. *J. Geophys. Res. Oceans: Oceans* **110**
695 (2005).
- 696 [60] Kunze, E., Firing, E., Hummon, J. M., Chereskin, T. K. & Thurnherr, A. M. Global abyssal mixing inferred
697 from lowered ADCP shear and CTD strain profiles. *J. Phys. Oceanogr.* **36**, 1553–1576 (2006).
- 698 [61] Whalen, C. B., Talley, L. D. & MacKinnon, J. A. Spatial and temporal variability of global ocean mixing
699 inferred from Argo profiles. *Geophys. Res. Lett.* **39** (2012).
- 700 [62] Waterhouse, A. F. *et al.* Global patterns of diapycnal mixing from measurements of the turbulent dissipation
701 rate. *J. Phys. Oceanogr.* 1854–1872 (2014).
- 702 [63] de Lavergne, C. *et al.* Toward global maps of internal tide energy sinks. *Ocean Modelling* **137**, 52–75 (2019).
- 703 [64] Egbert, G. D. & Ray, R. D. Estimates of m² tidal energy dissipation from TOPEX/Poseidon altimeter data.
704 *J. Geophys. Res. Oceans: Oceans* **106**, 22475–22502 (2001).
- 705 [65] Nakamura, T., Isoda, Y., Mitsudera, H., Takagi, S. & Nagasawa, M. Breaking of unsteady lee waves generated
706 by diurnal tides. *Geophys. Res. Lett.* **37** (2010).
- 707 [66] Nash, J. D. & Moum, J. N. Internal hydraulic flows on the continental shelf: High drag states over a small
708 bank. *J. Geophys. Res. Oceans: Oceans* **106**, 4593–4611 (2001).
- 709 [67] St. Laurent, L. & Garrett, C. The role of internal tides in mixing the deep ocean. *J. Phys. Oceanogr.* **32**,
710 2882–2899 (2002).
- 711 [68] Vic, C. *et al.* Deep-ocean mixing driven by small-scale internal tides. *Nat. Commun.* **10** (2019).

- 712 [69] Falahat, S., Nycander, J., Roquet, F. & Zarroug, M. Global calculation of tidal energy conversion into vertical
713 normal modes. *J. Phys. Oceanogr.* **44**, 3225–3244 (2014).
- 714 [70] Zhao, Z., Alford, M. H., Girton, J. B., Rainville, L. & Simmons, H. L. Global observations of open-ocean
715 mode-1 M2 internal tides. *J. Phys. Oceanogr.* **46**, 1657–1684 (2016).
- 716 [71] Polzin, K. Idealized solutions for the energy balance of the finescale internal wave field. *J. Phys. Oceanogr.* **34**,
717 231–246 (2004).
- 718 [72] Melet, A. *et al.* Internal tide generation by abyssal hills using analytical theory. *J. Geophys. Res. Oceans:*
719 *Oceans* **118**, 6303–6318 (2013).
- 720 [73] Goff, J. A. & Arbic, B. K. Global prediction of abyssal hill roughness statistics for use in ocean models from
721 digital maps of paleo-spreading rate, paleo-ridge orientation, and sediment thickness. *Ocean Modelling* **32**,
722 36–43 (2010).
- 723 [74] Lefauve, A., Muller, C. & Melet, A. A three-dimensional map of tidal dissipation over abyssal hills. *J. Geophys.*
724 *Res. Oceans: Oceans* **120**, 4760–4777 (2015).
- 725 [75] Polzin, K. L., Toole, J. M., Ledwell, J. R. & Schmitt, R. W. Spatial variability of turbulent mixing in the
726 abyssal ocean. *Science* **276**, 93–96 (1997).
- 727 [76] Ledwell, J. R. *et al.* Evidence for enhanced mixing over rough topography in the abyssal ocean. *Nature* **403**,
728 179–182 (2000).
- 729 [77] Muller, C. J. & Bühler, O. Saturation of the internal tides and induced mixing in the abyssal ocean. *J. Phys.*
730 *Oceanogr.* **39**, 2077–2096 (2009).
- 731 [78] Polzin, K. L. An abyssal recipe. *Ocean Modelling* **30**, 298–309 (2009).
- 732 [79] Klymak, J. M., Legg, S. & Pinkel, R. A simple parameterization of turbulent tidal mixing near supercritical
733 topography. *J. Phys. Oceanogr.* **40**, 2059–2074 (2010).
- 734 [80] Nikurashin, M. & Legg, S. A mechanism for local dissipation of internal tides generated at rough topography.
735 *J. Phys. Oceanogr.* **41**, 378–395 (2011).
- 736 [81] St. Laurent, L. C. & Nash, J. D. On the fraction of internal tide energy dissipated near topography. In *Pro-*
737 *ceedings of the 13th ‘Aha Huliko’ a Hawaiian Winter Workshop, Honolulu, HI, University of Hawaii at Manoa*
738 (2004).
- 739 [82] Klymak, J. M. *et al.* An estimate of tidal energy lost to turbulence at the Hawaiian Ridge. *J. Phys. Oceanogr.*
740 **36**, 1148–1164 (2006).

- 741 [83] Richet, O., Muller, C. & Chomaz, J.-M. Impact of a mean current on the internal tide energy dissipation at
742 the critical latitude. *J. Phys. Oceanogr.* **47**, 1457–1472 (2017).
- 743 [84] Dushaw, B. D., Howe, B. M., Cornuelle, B. D., Worcester, P. F. & Luther, D. S. Barotropic and baroclinic
744 tides in the central North Pacific Ocean determined from long-range reciprocal acoustic transmissions. *J. Phys.*
745 *Oceanogr.* **25**, 631–647 (1995).
- 746 [85] Ray, R. D. & Mitchum, G. T. Surface manifestation of internal tides generated near Hawaii. *Geophys. Res.*
747 *Lett.* **23**, 2101–2104 (1996).
- 748 [86] Zhao, Z. Mapping internal tides from satellite altimetry without blind directions. *J. Geophys. Res. Oceans:*
749 *Oceans* **124**, 8605–8625 (2019).
- 750 [87] Zhao, Z. The global mode-2 M2 internal tide. *J. Geophys. Res. Oceans: Oceans* **123**, 7725–7746 (2018).
- 751 [88] Alford, M. H. & Zhao, Z. Global patterns of low-mode internal-wave propagation. Part i: Energy and energy
752 flux. *J. Phys. Oceanogr.* **37**, 1829–1848 (2007).
- 753 [89] Zhao, Z., Alford, M. H., MacKinnon, J. A. & Pinkel, R. Long-range propagation of the semidiurnal internal
754 tide from the Hawaiian Ridge. *J. Phys. Oceanogr.* **40**, 713–736 (2010).
- 755 [90] Vic, C. *et al.* The lifecycle of semidiurnal internal tides over the northern mid-atlantic ridge. *J. Phys. Oceanogr.*
756 **48**, 61–80 (2018).
- 757 [91] Kelly, S., Jones, N., Nash, J. & Waterhouse, A. The geography of semidiurnal mode-1 internal-tide energy loss.
758 *Geophys. Res. Lett.* **40**, 4689–4693 (2013).
- 759 [92] Waterhouse, A. F. *et al.* Observations of the Tasman Sea internal tide beam. *J. Phys. Oceanogr.* **48**, 1283–1297
760 (2018).
- 761 [93] Müller, P. & Xu, N. Scattering of oceanic internal gravity waves off random bottom topography. *J. Phys.*
762 *Oceanogr.* **22**, 474–488 (1992).
- 763 [94] Bühler, O. & Holmes-Cerfon, M. Decay of an internal tide due to random topography in the ocean. *J. Fluid*
764 *Mech.* **678**, 271–293 (2011).
- 765 [95] Johnston, T. S. & Merrifield, M. A. Internal tide scattering at seamounts, ridges, and islands. *J. Geophys. Res.*
766 *Oceans: Oceans* **108** (2003).
- 767 [96] Mathur, M., Carter, G. S. & Peacock, T. Topographic scattering of the low-mode internal tide in the deep
768 ocean. *J. Geophys. Res. Oceans: Oceans* **119**, 2165–2182 (2014).

- 769 [97] Klymak, J. M., Buijsman, M., Legg, S. & Pinkel, R. Parameterizing surface and internal tide scattering and
770 breaking on supercritical topography: the one-and two-ridge cases. *J. Phys. Oceanogr.* **43**, 1380–1397 (2013).
- 771 [98] Johnston, T. S., Rudnick, D. L. & Kelly, S. M. Standing internal tides in the Tasman Sea observed by gliders.
772 *J. Phys. Oceanogr.* **45**, 2715–2737 (2015).
- 773 [99] Legg, S. & Adcroft, A. Internal wave breaking at concave and convex continental slopes. *J. Phys. Oceanogr.*
774 **33**, 2224–2246 (2003).
- 775 [100] Nash, J. D., Kunze, E., Toole, J. M. & Schmitt, R. W. Internal tide reflection and turbulent mixing on the
776 continental slope. *J. Phys. Oceanogr.* **34**, 1117–1134 (2004).
- 777 [101] Martini, K. I., Alford, M. H., Kunze, E., Kelly, S. M. & Nash, J. D. Internal bores and breaking internal tides
778 on the Oregon continental slope. *J. Phys. Oceanogr.* **43**, 120–139 (2013).
- 779 [102] Legg, S. Scattering of low-mode internal waves at finite isolated topography. *J. Phys. Oceanogr.* **44**, 359–383
780 (2014).
- 781 [103] Ansong, J. K. *et al.* Geographical distribution of diurnal and semidiurnal parametric subharmonic instability
782 in a global ocean circulation model. *J. Phys. Oceanogr.* **48**, 1409–1431 (2018).
- 783 [104] Hibiya, T. & Nagasawa, M. Latitudinal dependence of diapycnal diffusivity in the thermocline estimated using
784 a finescale parameterization. *Geophys. Res. Lett.* **31** (2004).
- 785 [105] Hazewinkel, J. & Winters, K. PSI of the internal tide on a β plane: flux divergence and near-inertial wave
786 propagation. *J. Phys. Oceanogr.* **41**, 1673–1682 (2011).
- 787 [106] Eden, C. & Olbers, D. An energy compartment model for propagation, nonlinear interaction, and dissipation
788 of internal gravity waves. *J. Phys. Oceanogr.* **44**, 2093–2106 (2014).
- 789 [107] Rainville, L. & Pinkel, R. Propagation of low-mode internal waves through the ocean. *J. Phys. Oceanogr.* **36**,
790 1220–1236 (2006).
- 791 [108] Polzin, K. L. Mesoscale Eddy-Internal Wave Coupling. Part I: Symmetry, Wave Capture, and Results from the
792 Mid-Ocean Dynamics Experiment. *J. Phys. Oceanogr.* **38**, 2556–2574 (2008).
- 793 [109] Polzin, K. L. Mesoscale Eddy-Internal Wave Coupling. Part II: Energetics and Results from PolyMode. *J. Phys.*
794 *Oceanogr.* **40**, 789–801 (2010).
- 795 [110] Kelly, S. M., Lermusiaux, P. F., Duda, T. F. & Haley Jr, P. J. A coupled-mode shallow-water model for tidal
796 analysis: internal tide reflection and refraction by the Gulf Stream. *J. Phys. Oceanogr.* **46**, 3661–3679 (2016).

- 797 [111] Buijsman, M. C. *et al.* Semidiurnal internal tide incoherence in the equatorial Pacific. *J. Geophys. Res. Oceans:*
798 *Oceans* **122**, 5286–5305 (2017).
- 799 [112] Dunphy, M., Ponte, A. L., Klein, P. & Le Gentil, S. Low-mode internal tide propagation in a turbulent eddy
800 field. *J. Phys. Oceanogr.* **47**, 649–665 (2017).
- 801 [113] Pollard, R. T. & Millard, R. C. Comparison between observed and simulated wind-generated inertial oscillations.
802 In *Deep Sea Research and Oceanographic Abstracts*, vol. 17, 813–821 (Elsevier, 1970).
- 803 [114] Alford, M. H. & Whitmont, M. Seasonal and spatial variability of near-inertial kinetic energy from historical
804 moored velocity records. *J. Phys. Oceanogr.* **37**, 2022–2037 (2007).
- 805 [115] Whalen, C. B., MacKinnon, J. A. & Talley, L. D. Large-scale impacts of the mesoscale environment on mixing
806 from wind-driven internal waves. *Nature Geosci.* **11**, 842–847 (2018).
- 807 [116] D’Asaro, E. A. *et al.* Upper-ocean inertial currents forced by a strong storm. I: Data and comparisons with
808 linear-theory. *J. Phys. Oceanogr.* **25**, 2909–2936 (1995).
- 809 [117] Price, J. F. Internal wave wake of a moving storm. Part I. Scales, energy budget and observations. *J. Phys.*
810 *Oceanogr.* **13**, 949–965 (1983).
- 811 [118] Church, J. A., Joyce, T. & Price, J. F. Current and density observations across the wake of Hurricane Gay. *J.*
812 *Phys. Oceanogr.* **19**, 259–265 (1989).
- 813 [119] Sanford, T. B., Price, J. F. & Girton, J. B. Upper-ocean response to hurricane frances (2004) observed by
814 profiling EM-APEX floats. *J. Phys. Oceanogr.* **41**, 1041–1056 (2011).
- 815 [120] Dohan, K. & Davis, R. E. Mixing in the transition layer during two storm events. *J. Phys. Oceanogr.* **41**, 42–66
816 (2011).
- 817 [121] Johnston, T. S. *et al.* Decay mechanisms of near-inertial mixed layer oscillations in the Bay of Bengal. *Oceanogr.*
818 **29**, 180–191 (2016).
- 819 [122] Gill, A. E. On the behavior of internal waves in the wakes of storms. *J. Phys. Oceanogr.* **14**, 1129–1151 (1984).
- 820 [123] Alford, M. H. Redistribution of energy available for ocean mixing by long-range propagation of internal waves.
821 *Nature* **423**, 159–162 (2003).
- 822 [124] Alford, M., Cronin, M. & Klymak, J. Annual cycle and depth penetration of wind-generated near-inertial
823 internal waves at Ocean Station Papa in the Northeast Pacific. *J. Phys. Oceanogr.* **42**, 889–909 (2012).
- 824 [125] Chaigneau, A., Pizarro, O. & Rojas, W. Global climatology of near-inertial current characteristics from La-
825 grangian observations. *Geophys. Res. Lett.* **35** (2008).

- 826 [126] Furuichi, N., Hibiya, T. & Niwa, Y. Model-predicted distribution of wind-induced internal wave energy in the
827 world's oceans. *J. Geophys. Res. Oceans: Oceans* **113** (2008).
- 828 [127] Zhai, X., Greatbatch, R. J., Eden, C. & Hibiya, T. On the loss of wind-induced near-inertial energy to turbulent
829 mixing in the upper ocean. *J. Phys. Oceanogr.* **39**, 3040–3045 (2009).
- 830 [128] Rimac, A., Storch, J.-S. v. & Eden, C. The total energy flux leaving the ocean's mixed layer. *J. Phys. Oceanogr.*
831 **46**, 1885–1900 (2016).
- 832 [129] Jouanno, J., Capet, X., Madec, G., Roulet, G. & Klein, P. Dissipation of the energy imparted by mid-latitude
833 storms in the Southern Ocean. *Ocean Sci.* **12**, 743–769 (2016).
- 834 [130] Weller, R. A. The relation of near-inertial motions observed in the mixed layer during the JASIN (1978)
835 experiment to the local wind stress and to the quasi-geostrophic flow field. *J. Phys. Oceanogr.* **12**, 1122–1136
836 (1982).
- 837 [131] Jing, Z., Wu, L. & Ma, X. Energy Exchange between the Mesoscale Oceanic Eddies and Wind-Forced Near-
838 Inertial Oscillations. *J. Phys. Oceanogr.* **47**, 721–733 (2017).
- 839 [132] Whitt, D. B. & Thomas, L. N. Resonant generation and energetics of wind-forced near-inertial motions in a
840 geostrophic flow. *J. Phys. Oceanogr.* **45**, 181–208 (2015).
- 841 [133] Van Meurs, P. Interactions between near-inertial mixed layer currents and the mesoscale: The importance of
842 spatial variabilities in the vorticity field. *J. Phys. Oceanogr.* **28**, 1363–1388 (1998).
- 843 [134] D'Asaro, E. A. Upper-ocean inertial currents forced by a strong storm. Part iii: Interaction of inertial currents
844 and mesoscale eddies. *J. Phys. Oceanogr.* **25**, 2953–2958 (1995).
- 845 [135] Elipot, S., Lumpkin, R. & Prieto, G. Modification of inertial oscillations by the mesoscale eddy field. *J. Geophys.*
846 *Res.-Oceans* **115** (2010).
- 847 [136] Simmons, H. L. & Alford, M. H. Simulating the long-range swell of internal waves generated by ocean storms.
848 *Oceanogr.* **25**, 30–41 (2012).
- 849 [137] Rimac, A., Storch, J.-S., Eden, C. & Haak, H. The influence of high-resolution wind stress field on the power
850 input to near-inertial motions in the ocean. *Geophys. Res. Lett.* **40**, 4882–4886 (2013).
- 851 [138] Alford, M. H. & Gregg, M. C. Near-inertial mixing: Modulation of shear, strain and microstructure at low
852 latitude. *J. Geophys. Res.-Oceans* **106**, 16947–16968 (2001).
- 853 [139] Watanabe, M. & Hibiya, T. Global estimates of the wind-induced energy flux to inertial motions in the surface
854 mixed layer. *Geophys. Res. Lett.* **29**, 64–1 (2002).

- 855 [140] Plueddemann, A. & Farrar, J. Observations and models of the energy flux from the wind to mixed-layer inertial
856 currents. *Deep-Sea Res. II* **53**, 5–30 (2006).
- 857 [141] Liu, G., Perrie, W. & Hughes, C. Surface wave effects on the wind-power input to mixed layer near-inertial
858 motions. *J. Phys. Oceanogr.* **47**, 1077–1093 (2017).
- 859 [142] Jiang, J., Lu, Y. & Perrie, W. Estimating the energy flux from the wind to ocean inertial motions: The
860 sensitivity to surface wind fields. *Geophys. Res. Lett.* **32** (2005).
- 861 [143] Alford, M. H. Improved global maps and 54-year history of wind-work on ocean inertial motions. *Geophys. Res.*
862 *Lett.* **30** (2003).
- 863 [144] Liu, Y., Jing, Z. & Wu, L. Wind power on oceanic near-inertial oscillations in the global ocean estimated from
864 surface drifters. *Geophys. Res. Lett.* **46**, 2647–2653 (2019).
- 865 [145] Alford, M. H., MacKinnon, J. A., Pinkel, R. & Klymak, J. M. Space–time scales of shear in the North Pacific.
866 *J. Phys. Oceanogr.* **47**, 2455–2478 (2017).
- 867 [146] Cuypers, Y., Le Vaillant, X., Bouruet-Aubertot, P., Vialard, J. & Mcphaden, M. J. Tropical storm-induced
868 near-inertial internal waves during the Cirene experiment: Energy fluxes and impact on vertical mixing. *J.*
869 *Geophys. Res. Oceans: Oceans* **118**, 358–380 (2013).
- 870 [147] Garrett, C. What is the “near-inertial” band and why is it different from the rest of the internal wave spectrum?
871 *J. Phys. Oceanogr.* **31**, 962–971 (2001).
- 872 [148] Jeon, C. *et al.* Poleward-propagating near-inertial waves enabled by the western boundary current. *Scientific*
873 *reports* **9** (2019).
- 874 [149] Nagasawa, M., Niwa, Y. & Hibiya, T. Spatial and temporal distribution of the wind-induced internal wave
875 energy available for deep water mixing in the North Pacific. *J. Geophys. Res. Oceans: Oceans* **105**, 13933–
876 13943 (2000).
- 877 [150] Komori, N., Ohfuchi, W., Taguchi, B., Sasaki, H. & Klein, P. Deep ocean inertia-gravity waves simulated in a
878 high-resolution global coupled atmosphere–ocean GCM. *Geophys. Res. Lett.* **35** (2008).
- 879 [151] Silverthorne, K. E. & Toole, J. M. Seasonal kinetic energy variability of near-inertial motions. *J. Phys. Oceanogr.*
880 **39**, 1035–1049 (2009).
- 881 [152] Inoue, R., Watanabe, M. & Osafune, S. Wind-induced mixing in the North Pacific. *J. Phys. Oceanogr.* **47**,
882 1587–1603 (2017).
- 883 [153] Kunze, E. Near-inertial wave-propagation in geostrophic shear. *J. Phys. Oceanogr.* **15**, 544–565 (1985).

- 884 [154] Young, W. & Jelloul, M. B. Propagation of near-inertial oscillations through a geostrophic flow. *J. Mar. Res.*
885 **55**, 735–766 (1997).
- 886 [155] Klein, P., Smith, S. L. & Lapeyre, G. Organization of near-inertial energy by an eddy field. *Q. J. Roy. Meteor.*
887 *Soc.* **130**, 1153–1166 (2004).
- 888 [156] Danioux, E., Klein, P. & Rivière, P. Propagation of wind energy into the deep ocean through a fully turbulent
889 mesoscale eddy field. *J. Phys. Oceanogr.* **38**, 2224–2241 (2008).
- 890 [157] Mooers, C. N. Several effects of a baroclinic current on the cross-stream propagation of inertial-internal waves.
891 *Geophys. Astro. Fluid.* **6**, 245–275 (1975).
- 892 [158] Whitt, D. & Thomas, L. Near-inertial waves in strongly baroclinic currents. *J. Phys. Oceanogr.* 706–725 (2013).
- 893 [159] Whitt, D. B., Thomas, L. N., Klymak, J. M., Lee, C. M. & D’Asaro, E. A. Interaction of superinertial waves
894 with submesoscale cyclonic filaments in the north wall of the Gulf Stream. *J. Phys. Oceanogr.* **48**, 81–99 (2018).
- 895 [160] Padman, L., Levine, M., Dillon, T., Morison, J. & Pinkel, R. Hydrography and microstructure of an Arctic
896 Cyclonic Eddy. *J. Geophys. Res.-Oceans* **95**, 9411–9420 (1990).
- 897 [161] Kunze, E. The energy-balance in a warm-core rings near-inertial critical layer. *J. Phys. Oceanogr.* **25**, 942–957
898 (1995).
- 899 [162] Joyce, T., Toole, J., Klein, P. & Thomas, L. A Near-Inertial Mode observed within a Gulf Stream Warm-Core
900 Ring. *J. Geophys. Res.* (2013).
- 901 [163] Sheen, K. *et al.* Modification of turbulent dissipation rates by a deep Southern Ocean eddy. *Geophys. Res. Lett.*
902 (2015).
- 903 [164] Fer, I., Bosse, A., Ferron, B. & Bouruet-Aubertot, P. The dissipation of kinetic energy in the Lofoten Basin
904 Eddy. *J. Phys. Oceanogr.* **48**, 1299–1316 (2018).
- 905 [165] Wunsch, C. The work done by the wind on the oceanic general circulation. *J. Phys. Oceanogr.* **28**, 2332–2340
906 (1998).
- 907 [166] von Storch, J.-S., Sasaki, H. & Marotzke, J. Wind-generated power input to the deep ocean: An estimate using
908 a 1/10 general circulation model. *J. Phys. Oceanogr.* **37**, 657–672 (2007).
- 909 [167] Arbic, B. K. & Flierl, G. R. Baroclinically unstable geostrophic turbulence in the limits of strong and weak
910 bottom Ekman friction: Application to midocean eddies. *J. Phys. Oceanogr.* **34**, 2257–2273 (2004).
- 911 [168] Sen, A., Scott, R. B. & Arbic, B. K. Global energy dissipation rate of deep-ocean low-frequency flows by
912 quadratic bottom boundary layer drag: Computations from current-meter data. *Geophys. Res. Lett.* **35** (2008).

- 913 [169] Klymak, J. M. Nonpropagating form drag and turbulence due to stratified flow over large-scale abyssal hill
914 topography. *J. Phys. Oceanogr.* **48**, 2383–2395 (2018).
- 915 [170] Renault, L. *et al.* Modulation of wind work by oceanic current interaction with the atmosphere. *J. Phys.*
916 *Oceanogr.* **46**, 1685–1704 (2016).
- 917 [171] Nikurashin, M. & Ferrari, R. Global energy conversion rate from geostrophic flows into internal lee waves in
918 the deep ocean. *Geophys. Res. Lett.* **38** (2011).
- 919 [172] Scott, R. B., Goff, J. A., Naveira Garabato, A. & Nurser, A. Global rate and spectral characteristics of internal
920 gravity wave generation by geostrophic flow over topography. *J. Geophys. Res. Oceans: Oceans* **116** (2011).
- 921 [173] Wright, C. J., Scott, R. B., Ailliot, P. & Furnival, D. Lee wave generation rates in the deep ocean. *Geophys.*
922 *Res. Lett.* **41**, 2434–2440 (2014).
- 923 [174] Nikurashin, M., Ferrari, R., Grisouard, N. & Polzin, K. The impact of finite-amplitude bottom topography on
924 internal wave generation in the Southern Ocean. *J. Phys. Oceanogr.* **44**, 2938–2950 (2014).
- 925 [175] Yang, L., Nikurashin, M., Hogg, A. M. & Sloyan, B. M. Energy loss from transient eddies due to lee wave
926 generation in the Southern Ocean. *J. Phys. Oceanogr.* **48**, 2867–2885 (2018).
- 927 [176] Melet, A., Hallberg, R., Adcroft, A., Nikurashin, M. & Legg, S. Energy flux into internal lee waves: sensitivity
928 to future climate changes using linear theory and a climate model. *J. Clim.* **28**, 2365–2384 (2015).
- 929 [177] Zheng, K. & Nikurashin, M. Downstream propagation and remote dissipation of internal waves in the southern
930 ocean. *J. Phys. Oceanogr.* **49**, 1873–1887 (2019).
- 931 [178] Waterman, S., Garabato, A. C. N. & Polzin, K. L. Internal Waves and Turbulence in the Antarctic Circumpolar
932 Current. *J. Phys. Oceanogr.* **43**, 259–282 (2013).
- 933 [179] Sheen, K. L. *et al.* Rates and mechanisms of turbulent dissipation and mixing in the Southern Ocean: Results
934 from the Diapycnal and Isopycnal Mixing Experiment in the Southern Ocean (DIMES). *J. Geophys. Res.:
935 Oceans* **118**, 2774–2792 (2013).
- 936 [180] Meyer, A., Sloyan, B. M., Polzin, K. L., Phillips, H. E. & Bindoff, N. L. Mixing variability in the Southern
937 Ocean. *J. Phys. Oceanogr.* **45**, 966–987 (2015).
- 938 [181] Cusack, J. M., Naveira Garabato, A. C., Smeed, D. A. & Girton, J. B. Observation of a large lee wave in the
939 Drake Passage. *J. Phys. Oceanogr.* **47**, 793–810 (2017).
- 940 [182] Clement, L., Frajka-Williams, E., Sheen, K., Brearley, J. & Garabato, A. N. Generation of internal waves by
941 eddies impinging on the western boundary of the North Atlantic. *J. Phys. Oceanogr.* **46**, 1067–1079 (2016).

- 942 [183] Brearley, J. A., Sheen, K. L., Naveira Garabato, A. C., Smeed, D. A. & Waterman, S. Eddy-induced modulation
943 of turbulent dissipation over rough topography in the Southern Ocean. *J. Phys. Oceanogr.* **43**, 2288–2308 (2013).
- 944 [184] Köhler, J. *et al.* Variability in the internal wave field induced by the Atlantic Deep Western Boundary Current
945 at 16 N. *J. Phys. Oceanogr.* **44**, 492–516 (2014).
- 946 [185] Sheen, K. *et al.* Eddy-induced variability in Southern Ocean abyssal mixing on climatic timescales. *Nature*
947 *Geosci.* **7**, 577–582 (2014).
- 948 [186] Kunze, E. & Lien, R.-C. Energy sinks for lee waves in shear flow. *J. Phys. Oceanogr.* (2019).
- 949 [187] Naveira Garabato, A. C., Polzin, K. L., King, B. A., Heywood, K. J. & Visbeck, M. Widespread intense
950 turbulent mixing in the Southern Ocean. *Science* **303**, 210–213 (2004).
- 951 [188] St. Laurent, L. *et al.* Turbulence and diapycnal mixing in Drake Passage. *J. Phys. Oceanogr.* **42**, 2143–2152
952 (2012).
- 953 [189] Alford, M. H. *et al.* Turbulent mixing and hydraulic control of abyssal water in the Samoan Passage. *Geophys.*
954 *Res. Lett.* **40**, 4668–4674 (2013).
- 955 [190] Thurnherr, A. Diapycnal mixing associated with an overflow in a deep submarine canyon. *Deep-Sea Res.*
956 *Oceanogr. Abstr.* **53**, 194–206 (2006).
- 957 [191] Nikurashin, M. & Ferrari, R. Radiation and dissipation of internal waves generated by geostrophic motions
958 impinging on small-scale topography: Theory. *J. Phys. Oceanogr.* **40**, 1055–1074 (2010).
- 959 [192] Trossman, D. S. *et al.* Internal lee wave closures: Parameter sensitivity and comparison to observations. *J.*
960 *Geophys. Res. Oceans: Oceans* **120**, 7997–8019 (2015).
- 961 [193] Griffiths, M. & Reeder, M. J. Stratospheric inertia–gravity waves generated in a numerical model of frontoge-
962 nesis. I: Model solutions. *Q. J. Roy. Meteor. Soc.* **122**, 1153–1174 (1996).
- 963 [194] Reeder, M. J. & Griffiths, M. Stratospheric inertia–gravity waves generated in a numerical model of frontoge-
964 nesis. II: Wave sources, generation mechanisms and momentum fluxes. *Q. J. Roy. Meteor. Soc.* **122**, 1175–1195
965 (1996).
- 966 [195] Danioux, E., Vanneste, J., Klein, P. & Sasaki, H. Spontaneous inertia-gravity-wave generation by surface-
967 intensified turbulence. *J. Fluid Mech.* **699**, 153–173 (2012).
- 968 [196] Vanneste, J. Balance and spontaneous wave generation in geophysical flows. *Ann. Rev. Fluid Mech.* (2013).
- 969 [197] Snyder, C., Skamarock, W. C. & Rotunno, R. Frontal dynamics near and following frontal collapse. *J. Atmos.*
970 *Sci.* **50**, 3194–3212 (1993).

- 971 [198] Nagai, T., Tandon, A., Kunze, E. & Mahadevan, A. Spontaneous generation of near-inertial waves by the
972 Kuroshio Front. *J. Phys. Oceanogr.* **45**, 2381–2406 (2015).
- 973 [199] Shakespeare, C. J. & Hogg, A. M. Spontaneous surface generation and interior amplification of internal waves
974 in a regional-scale ocean model. *J. Phys. Oceanogr.* **47**, 811–826 (2017).
- 975 [200] Rossby, C. On the mutual adjustment of pressure and velocity distributions in certain simple current systems.
976 *J. Mar. Res* **1**, 280 (1937).
- 977 [201] Ford, R. Gravity wave radiation from vortex trains in rotating shallow water. *J. Fluid Mech.* **281**, 81–118
978 (1994).
- 979 [202] Xie, J.-H. & Vanneste, J. A generalised-Lagrangian-mean model of the interactions between near-inertial waves
980 and mean flow. *J. Fluid Mech.* **774**, 143–169 (2015).
- 981 [203] Wagner, G. & Young, W. A three-component model for the coupled evolution of near-inertial waves, quasi-
982 geostrophic flow and the near-inertial second harmonic. *J. Fluid Mech.* **802**, 806–837 (2016).
- 983 [204] Thomas, L. N. On the effects of frontogenetic strain on symmetric instability and inertia–gravity waves. *J.*
984 *Fluid Mech.* **711**, 620–640 (2012).
- 985 [205] Alford, M. H., Shcherbina, A. Y. & Gregg, M. C. Observations of near-inertial internal gravity waves radiating
986 from a frontal jet. *J. Phys. Oceanogr.* **43**, 1225–1239 (2013).
- 987 [206] Ferrari, R. & Wunsch, C. The distribution of eddy kinetic and potential energies in the global ocean. *Tellus*
988 *Series a-Dynamic Meteorology and Oceanography* **62**, 92–108 (2010).
- 989 [207] Shakespeare, C. J. & Hogg, A. The life cycle of spontaneously generated internal waves. *J. Phys. Oceanogr.* **48**,
990 343–359 (2018).
- 991 [208] Toggweiler, J. & Samuels, B. On the ocean’s large-scale circulation near the limit of no vertical mixing. *J. Phys.*
992 *Oceanogr.* **28**, 1832–1852 (1998).
- 993 [209] Oka, A. & Niwa, Y. Pacific deep circulation and ventilation controlled by tidal mixing away from the sea
994 bottom. *Nat. Commun.* **4**, 2419 (2013).
- 995 [210] Melet, A., Legg, S. & Hallberg, R. Climatic impacts of parameterized local and remote tidal mixing. *J. Clim.*
996 **29**, 3473–3500 (2016).
- 997 [211] Hieronymus, M., Nycander, J., Nilsson, J., Döös, K. & Hallberg, R. Oceanic overturning and heat transport:
998 The role of background diffusivity. *J. Clim.* **32**, 701–716 (2019).

- 999 [212] Adcroft, A., Scott, J. R. & Marotzke, J. Impact of geothermal heating on the global ocean circulation. *Geophys.*
1000 *Res. Lett.* **28**, 1735–1738 (2001).
- 1001 [213] Emile-Geay, J. & Madec, G. Geothermal heating, diapycnal mixing and the abyssal circulation. *Ocean Science*
1002 **5**, 203–217 (2009).
- 1003 [214] Naveira Garabato, A. C. *et al.* Rapid mixing and exchange of deep-ocean waters in an abyssal boundary current.
1004 *Proc. Natl. Acad. Sci. U.S.A.* (2019).
- 1005 [215] Bryden, H. L. & Nurser, A. G. Effects of strait mixing on ocean stratification. *J. Phys. Oceanogr.* **33**, 1870–1872
1006 (2003).
- 1007 [216] Ganachaud, A. Large-scale mass transports, water mass formation, and diffusivities estimated from World
1008 Ocean Circulation Experiment (WOCE) hydrographic data. *J. Geophys. Res. Oceans: Oceans* **108** (2003).
- 1009 [217] Lumpkin, R. & Speer, K. Global ocean meridional overturning. *J. Phys. Oceanogr.* **37**, 2550–2562 (2007).
- 1010 [218] Jayne, S. R. The impact of abyssal mixing parameterizations in an ocean general circulation model. *J. Phys.*
1011 *Oceanogr.* **39**, 1756–1775 (2009).
- 1012 [219] De Lavergne, C., Madec, G., Le Sommer, J., Nurser, A. G. & Naveira Garabato, A. C. The impact of a variable
1013 mixing efficiency on the abyssal overturning. *J. Phys. Oceanogr.* **46**, 663–681 (2016).
- 1014 [220] Melet, A., Hallberg, R., Legg, S. & Nikurashin, M. Sensitivity of the ocean state to lee wave-driven mixing. *J.*
1015 *Phys. Oceanogr.* **44**, 900–921 (2014).
- 1016 [221] Saenko, O. & Merryfield, W. On the effect of topographically enhanced mixing on the global ocean circulation.
1017 *J. Phys. Oceanogr.* **35**, 826–834 (2005).
- 1018 [222] Simmons, H. L., Jayne, S. R., Laurent, L. C. S. & Weaver, A. J. Tidally driven mixing in a numerical model of
1019 the ocean general circulation. *Ocean Modelling* **6**, 245–263 (2004).
- 1020 [223] Melet, A., Hallberg, R., Legg, S. & Polzin, K. Sensitivity of the ocean state to the vertical distribution of
1021 internal-tide-driven mixing. *J. Phys. Oceanogr.* **43**, 602–615 (2013).
- 1022 [224] Tatebe, H., Tanaka, Y., Komuro, Y. & Hasumi, H. Impact of deep ocean mixing on the climatic mean state in
1023 the Southern Ocean. *Scientific reports* **8**, 14479 (2018).
- 1024 [225] Zhu, Y. & Zhang, R.-H. A modified vertical mixing parameterization for its improved ocean and coupled
1025 simulations in the tropical Pacific. *J. Phys. Oceanogr.* **49**, 21–37 (2019).
- 1026 [226] Jochum, M. *et al.* The impact of oceanic near-inertial waves on climate. *J. Clim.* **26**, 2833–2844 (2013).

- 1027 [227] Stanley, G. J. & Saenko, O. A. Bottom-enhanced diapycnal mixing driven by mesoscale eddies: Sensitivity to
1028 wind energy supply. *J. Phys. Oceanogr.* **44**, 68–85 (2014).
- 1029 [228] Koch-Larrouy, A., Lengaigne, M., Terray, P., Madec, G. & Masson, S. Tidal mixing in the Indonesian seas and
1030 its effect on the tropical climate system. *Climate Dynamics* **34**, 891–904 (2010).
- 1031 [229] Kida, S. & Wijffels, S. The impact of the Indonesian Throughflow and tidal mixing on the summertime sea
1032 surface temperature in the western Indonesian seas. *J. Geophys. Res. Oceans: Oceans* **117** (2012).
- 1033 [230] Sasaki, H., Kida, S., Furue, R., Nonaka, M. & Masumoto, Y. An increase of the Indonesian Throughflow by
1034 internal tidal mixing in a high-resolution quasi-global ocean simulation. *Geophys. Res. Lett.* **45**, 8416–8424
1035 (2018).
- 1036 [231] Saenko, O. A., Zhai, X., Merryfield, W. J. & Lee, W. G. The combined effect of tidally and eddy-driven
1037 diapycnal mixing on the large-scale ocean circulation. *J. Phys. Oceanogr.* **42**, 526–538 (2012).
- 1038 [232] Munday, D., Allison, L., Johnson, H. & Marshall, D. Remote forcing of the Antarctic Circumpolar Current by
1039 diapycnal mixing. *Geophys. Res. Lett.* **38** (2011).
- 1040 [233] Savva, M. A. & Vanneste, J. Scattering of internal tides by barotropic quasigeostrophic flows. *J. Fluid Mech.*
1041 **856**, 504–530 (2018).
- 1042 [234] Zaron, E. D. Topographic and frictional controls on tides in the sea of Okhotsk. *Ocean Modelling* **117**, 1–11
1043 (2017).
- 1044 [235] Alford, M. H., Simmons, H. L., Marques, O. B. & Girton, J. B. Internal tide attenuation in the North Pacific.
1045 *Geophys. Res. Lett.* **46**, 8205–8213 (2019).
- 1046 [236] Naveira Garabato, A. C., Nurser, A. G., Scott, R. B. & Goff, J. A. The impact of small-scale topography on
1047 the dynamical balance of the ocean. *J. Phys. Oceanogr.* **43**, 647–668 (2013).
- 1048 [237] Klymak, J. M., Pinkel, R. & Rainville, L. Direct breaking of the internal tide near topography: Kaena ridge,
1049 Hawaii. *J. Phys. Oceanogr.* **38**, 380–399 (2008).
- 1050 [238] Zhao, Z. *et al.* Decomposition of the multimodal multidirectional M2 internal tide field. *J. Atmos. Ocean.*
1051 *Technol.* **36**, 1157–1173 (2019).

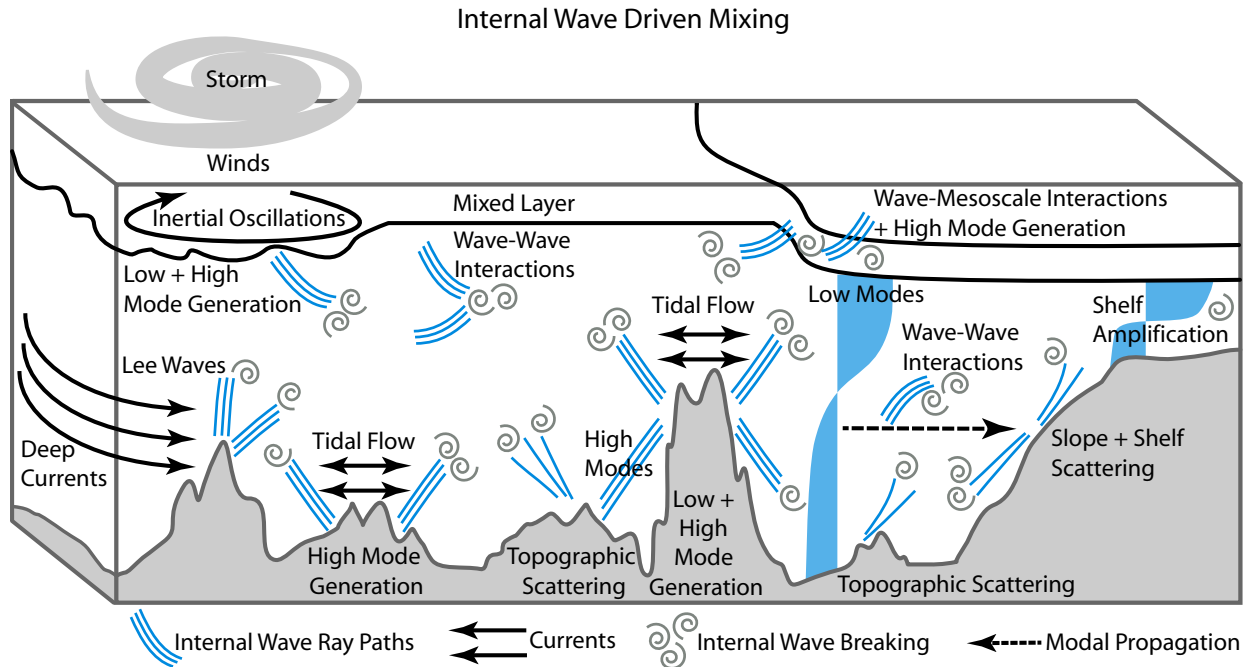


FIGURE 1. The primary internal wave mechanisms leading to ocean mixing.

Tides flow over many forms of topography, from abyssal hills to tall steep ridges, generating both high-mode and low-mode internal waves. Time-varying winds cause near-inertial oscillations in the mixed layer, radiating high- and low-mode internal waves. Lee waves are generated when deep currents impinge on topographic features. Time-varying surface currents can also generate internal waves. Both high and low modes propagate, undergo wave-wave interactions, and scatter off topographic features, eventually leading to dissipation. Low modes generated in the open ocean can also propagate and dissipate on continental slopes and shelves. Modified from Ref [21].

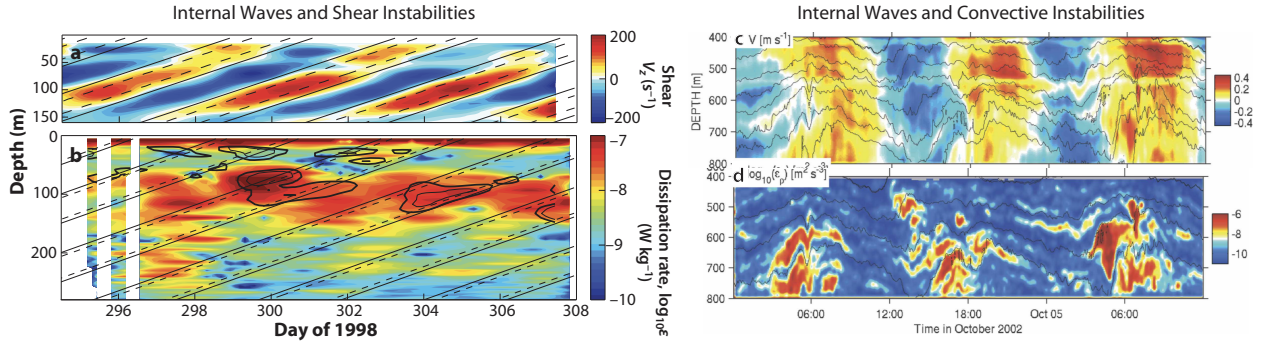


FIGURE 2. **Turbulent mixing in two different internal wave environments.** Meridional component of vertical shear (a) and dissipation rate (b) in the presence of a near-inertial internal wave from Ref [138]. Elevated dissipation rates are associated with strong vertical shear in the internal wave field, and turbulent mixing is attributed to shear instabilities. Adapted from Meridional velocity (c) and dissipation rate (d) during tidal flow over the Hawaiian ridge from Ref [237]. Peaks in the dissipation rate are in phase with the tidal cycle and are indicative of convective instabilities.

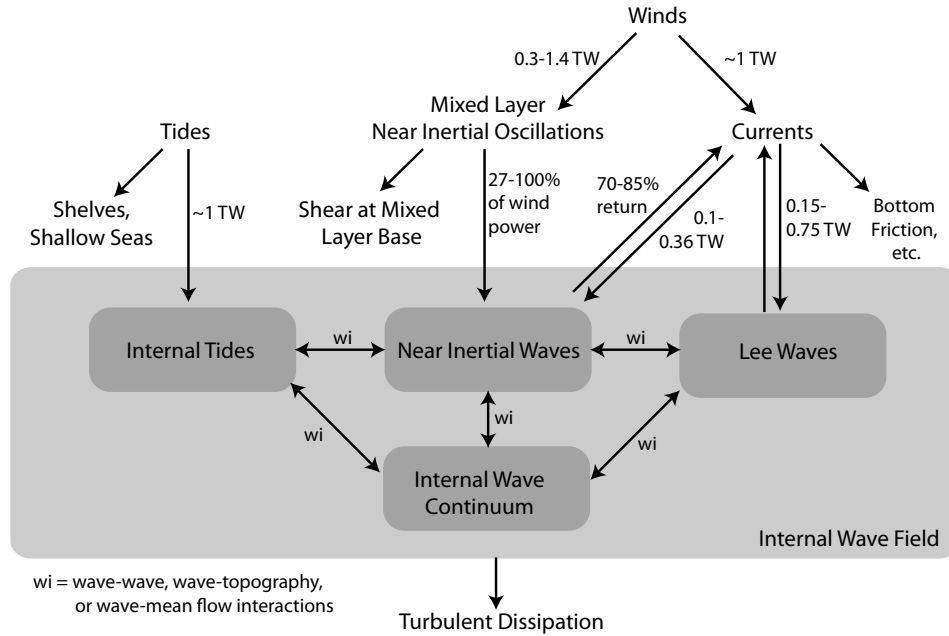


FIGURE 3. A simplified global energy budget of internal waves. Included are the sources of internal wave energy and the pathways of energy transfer until it is dissipated through turbulence. References for numbers quantifying energy transfers are provided in the main text.

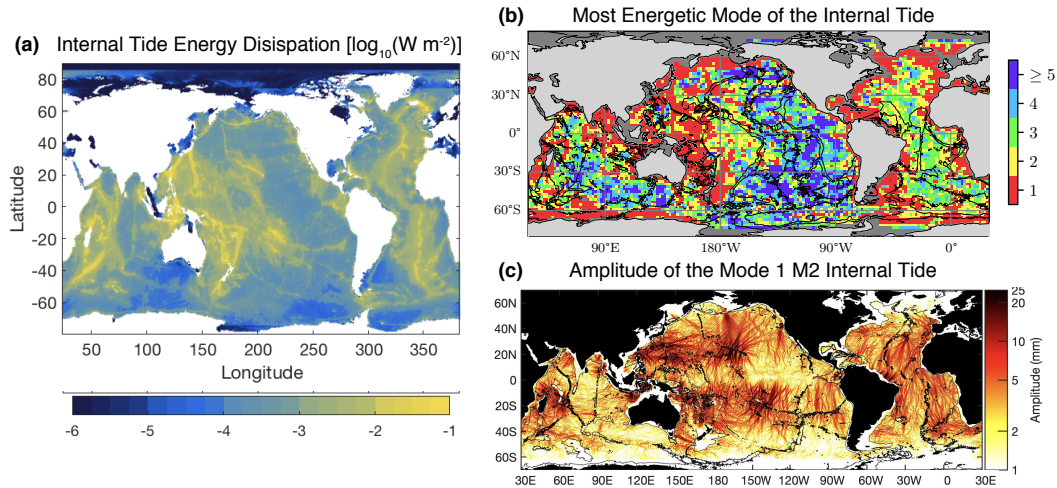


FIGURE 4. **The lifecycle of internal tides, including generation, propagation, and turbulent dissipation.** (a) A global map of the dissipation of the internal tide from a modelling study modified from Ref [63], (b) The most energetic mode (that is, vertical length scale) of internal tide generation varies throughout the globe, depending primarily on the geometry of the seafloor from Ref [68]. (c) The propagation of the first mode (the largest vertical length scale) M_2 internal tide can be tracked using sea surface height from altimetry up to thousands of kilometers away from the steep topographic generation sites [70] using an updated model [238] as explained in Ref [86].

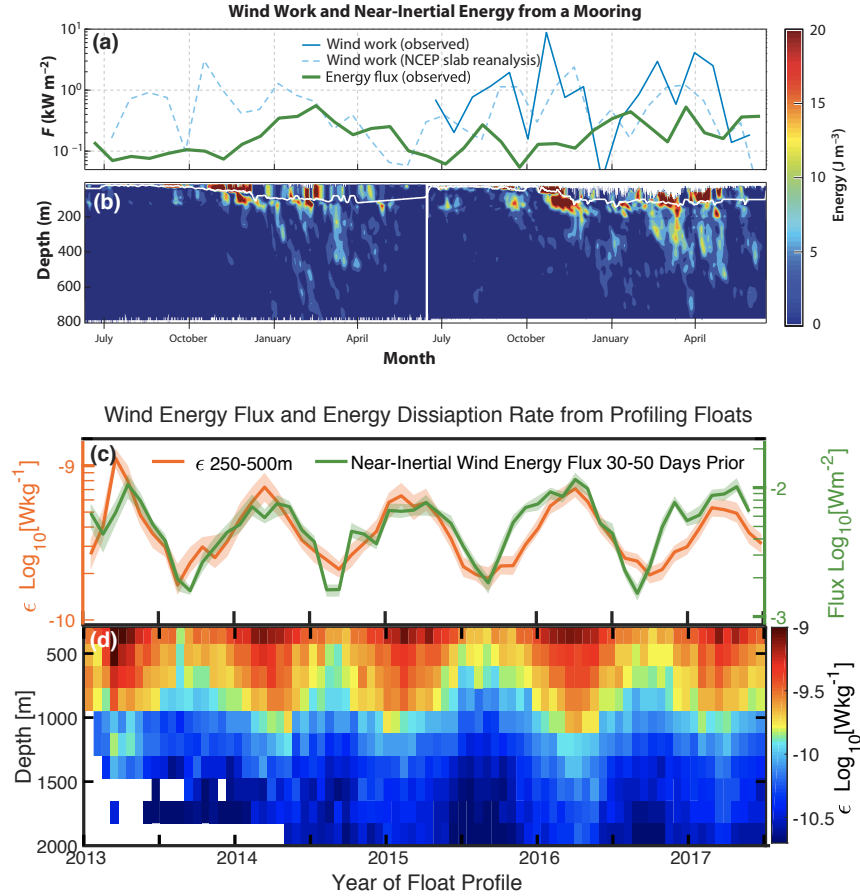


FIGURE 5. The seasonal cycle in wind activity tracks the seasonal cycle in near-inertial wave energy and dissipation rate in the North Pacific. (a-b) Mooring data show that the wind energy input into the mixed layer is elevated in the winter months, followed by an invigoration of the near-inertial internal wave field in the thermocline below, suggesting that the mixed layer oscillations radiate near-inertial internal waves (Modified from Ref[124]). A fraction of these waves will undergo turbulent dissipation locally. In fact, (c-d) the energy dissipation rate estimated using profiling float data also peaks in the winter, (c) lagging the wind energy flux from Ref [115].

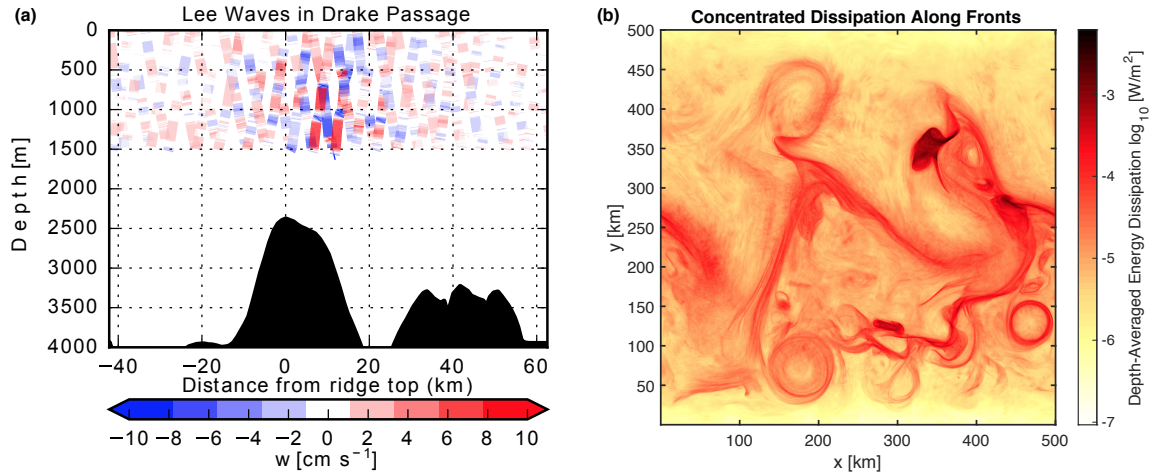


FIGURE 6. **Two mechanisms for internal wave generation from geographic current.** (a) Vertical velocity associated with lee waves in Drake Passage observed using profiling floats. (b) The vertically integrated energy dissipation in a high-resolution ocean model. Internal waves generated at fronts preferentially dissipate along those fronts. (a) Is from Ref [181] and (b) is modified from Ref [207].

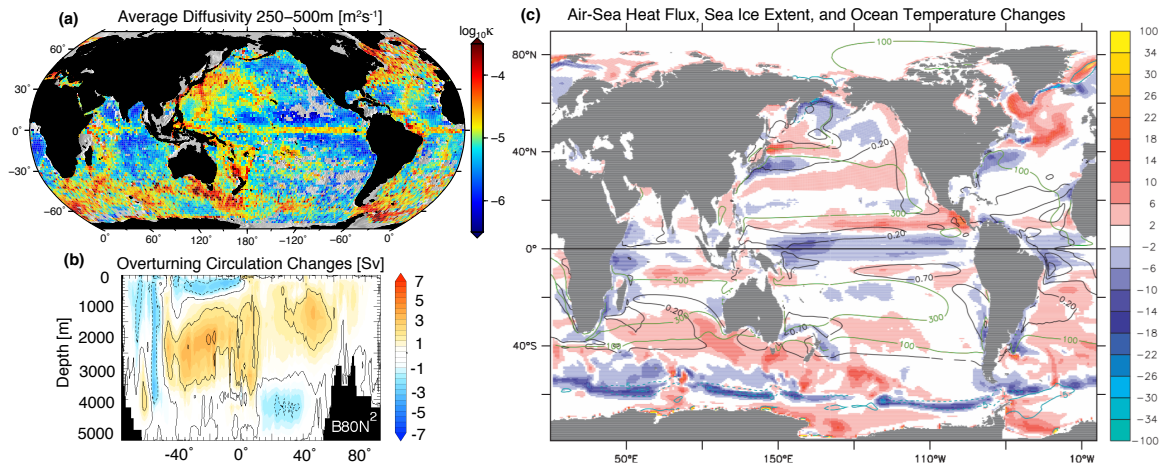


FIGURE 7. Global diapycnal mixing from internal waves and implications for circulation and climate. (a) The diffusivity estimated from profiling floats averaged between 250-500 m exhibits large geographic variability throughout the ocean (modified from Ref [115]). (b) The overturning circulation changes significantly when far-field tidal mixing is assigned to the basins compared to distributed across the basins, continental slopes and shelves (modified from Ref [210]). (c) Adding diffusivity from wind-generated near-inertial waves changes the downward surface heat flux (colors), sea ice extent (blue lines) and temperature on the 26 kg m^{-3} density surface (black line). The depth of 26 kg m^{-3} density surface is contoured in green, modified from Ref [226].